forests

MDPI

Article

Performance of Four Optical Methods in Estimating Leaf Area Index at Elementary Sampling Unit of *Larix principis-rupprechtii* Forests

Jie Zou [1,2,*], Yong Zuo [1,2], Peihong Zhong [1,2], Wei Hou [1,2], Peng Leng [1,2] and Bin Chen [3]

1 Spatial Information Research Center of Fujian Province, Fuzhou University, Fuzhou 350116, China; zuoyong209@163.com (Y.Z.); zhongpeihongfz@163.com (P.Z.); hwzb123@163.com (W.H.); lengpeng_lp@163.com (P.L.)
2 Key Laboratory of Spatial Data Mining and Information Sharing, Ministry of Education, Fuzhou 350116, China
3 Key Laboratory of Ecosystem Network Observation and Modeling, Institute of Geographic Sciences and Natural Resources Research, Chinese Academy of Sciences, Beijing 100101, China; chenbin@igsnrr.ac.cn
* Correspondence: zoujie@fzu.edu.cn; Tel.: +86-591-6317-9702

Received: 6 November 2019; Accepted: 18 December 2019; Published: 24 December 2019

Abstract: Optical methods are frequently used as a routine method to obtain the elementary sampling unit (ESU) leaf area index (LAI) of forests. However, few studies have attempted to evaluate whether the ESU LAI obtained from optical methods matches the accuracy required by the LAI map product validation community. In this study, four commonly used optical methods, including digital hemispherical photography (DHP), digital cover photography (DCP), tracing radiation of canopy and architecture (TRAC) and multispectral canopy imager (MCI), were adopted to estimate the ESU (25 m × 25 m) LAI of five *Larix principis-rupprechtii* forests with contrasting structural characteristics. The impacts of three factors, namely, inversion model, canopy element or woody components clumping index (Ω_e or Ω_w) algorithm, and the woody components correction method, on the ESU LAI estimation of the four optical methods were analyzed. Then, the LAI derived from the four optical methods was evaluated using the LAI obtained from litter collection measurements. Results show that the performance of the four optical methods in estimating the ESU LAI of the five forests was largely affected by the three factors. The accuracy of the LAI obtained from the DHP and MCI strongly relied on the inversion model, the Ω_e or Ω_w algorithm, and the woody components correction method adopted in the estimation. Then the best Ω_e or Ω_w algorithm, inversion model and woody components correction method to be used to obtain the ESU LAI of *L. principis-rupprechtii* forests with the smallest root mean square error (RMSE) and mean absolute error (MAE) were identified. Amongst the three typical woody components correction methods evaluated in this study, the woody-to-total area ratio obtained from the destructive measurements is the most effective method for DHP to derive the ESU LAI with the smallest RMSE and MAE. In contrast, using the woody area index obtained from the leaf-off DHP or DCP images as the woody components correction method would result in a large LAI underestimation. TRAC and MCI outperformed DHP and DCP in the ESU LAI estimation of the five forests, with the smallest RMSE and MAE. All the optical methods, except DCP, are qualified to obtain the ESU LAI of *L. principis-rupprechtii* forests with an MAE of <20% that is required by the global climate observation system. None of the optical methods, except TRAC, show the potential to obtain the ESU LAI of *L. principis-rupprechtii* forests with an MAE of <5%.

Keywords: leaf area index; clumping effects; inversion model; woody components correction method; *Larix*-dominated forest plots; optical method; elementary sampling unit

1. Introduction

Leaf area index (LAI) quantifies the number of leaves in an ecosystem [1] and is a key variable for describing the biophysical and physiological processes of vegetation–atmosphere interactions, including photosynthesis, respiration, energy exchange, and transpiration. Therefore, LAI is widely used in the fields of climate, forestry, and global change. For example, LAI is listed as one of the 16 essential climate variables required by the global climate observing system (GCOS) [2]. Remote sensing is an efficient and effective method of obtaining the global scale LAI maps required by GCOS. Several global scale LAI map products have been published in the past two decades, including CYCLOPES [3], ECOCLIMAP [4], GLOBCARBON [5], GLASS [6], MODIS [7,8], and GEOV1 [9]. However, large numerical value differences were found between the published LAI map products [10–13]. Compared with the remote sensing method, the ground-based LAI measurements which are usually obtained from optical methods (e.g., digital cover photography (DCP), digital hemispherical photography (DHP), LAI-2000/LAI-2200 (LI-COR, Lincoln, NE, USA), multispectral canopy imager (MCI) [14], and tracing radiation of canopy and architecture (TRAC) (3rd Wave Engineering, Winnipeg, Manitoba, Canada)) or direct methods (e.g., destructive measurements, litter collection, and allometric equations) at the elementary sampling unit (ESU) or pixel scale are usually regarded as accurate estimates and applied to validate the accuracy of LAI map products. Therefore, the accurate ground-based ESU LAI measurements of typical vegetation plots are essential in ensuring that the accuracy of the LAI map products matches the accuracy requirements of GCOS, i.e., the LAI product values must be within 20% of the ground-based LAI measurements and improved within 5% in the future [2,15].

Optical methods are usually chosen amongst indirect methods as the routine method to derive the ESU LAI of forests due to its high efficiency, low cost, and non-destructiveness to canopies [14,16]. Previous studies reported that the ESU LAI estimation of forests for optical methods is mainly affected by six estimation error sources, including clumping effects, overestimation of woody components, inversion model, sampling scheme, terrain slope, and observation conditions [16–19]. Progress to correct the six LAI estimation error sources has been achieved recently [15,19–22]. For example, Zou et al. [19] attempted to evaluate the performance of seven inversion models in the ESU plant and woody area index (PAI and WAI) estimations of forests and recommended three inversion models. Cao et al. [22] suggested three solutions to correct the influence of slope on the ESU LAI estimation of forests from DHP. Several studies have attempted to correct the overestimation of woody components on the ESU LAI estimation of forests by determining the woody-to-total area ratio or WAI through MCI [14,23], DHP [24], and terrestrial laser scanner [25,26]. However, few studies have attempted to evaluate whether these optical methods or solutions are effective in obtaining the ESU LAI of forests with estimation errors of <20% or 5% required by GCOS, especially for *Larix principis-rupprechtii* forests.

A field LAI measurement dataset called "Direct" (http://calvalportal.ceos.org/web/olive/site-description) is commonly used for validating global LAI map products [11,27]. The "Direct" dataset was collected from the datasets of several international field campaigns named Validation Land European Remote Sensing Instruments [28], Bigfoot [29], and the Southern African Regional Science Initiative 2000 [30]. However, previous studies pointed out that several estimation errors exist for the ESU LAI measurements of "Direct" [11,27]. Firstly, the majority of ESU LAI measurements were obtained without considering the overestimation of woody components on the LAI estimation and terrain slope. Secondly, the clumping effects of forest canopies were not accurately corrected as the variation of the canopy element clumping index (Ω_e) with zenith angles (θ) was not considered. Moreover, several Ω_e algorithms were adopted in the LAI estimation. However, a large difference was observed between the Ω_e derived from different Ω_e estimation methods using the same Ω_e algorithm or from different Ω_e algorithms with the same Ω_e estimation method [19,31–33]. Thirdly, various inversion models and indirect methods were used in the ESU LAI estimation. However, previous studies reported that large differences were observed between the LAI derived from different inversion models and indirect methods [19,34,35]. Therefore, an accurate and reliable solution to measure the ESU LAI of forests that matches the accuracy requirements of GCOS is essential to the LAI map product

validation community. The land product validation group of the Committee on Earth Observation Satellites published a guideline to validate global LAI map products [2]. However, the solution to obtain an accurate ESU LAI of forests was not given enough detail in the guideline, especially the solution to reduce or remove the six LAI estimation error sources of optical methods. Additional works must still be conducted to achieve accurate ESU LAI measurements that match the accuracy requirements of GCOS.

The goal of this study is to determine whether the four commonly used optical methods (e.g., DCP, DHP, TRAC, and MCI) are qualified to obtain the ESU LAI of *L. principis-rupprechtii* forests with estimation errors of <20% or 5% required by GCOS. To achieve this goal, four commonly used inversion models and three Ω_e or woody components clumping index (Ω_w) algorithms were adopted in the LAI estimation. Moreover, the impact of the three schemes for removing the overestimation of woody components on the LAI estimation was analyzed. The LAIs obtained from the four optical methods were compared with the LAI obtained using the litter collection measurements. Finally, we attempted to determine whether the four optical methods can provide ESU LAI measurements with an accuracy that matches the requirements of GCOS and the best solution to derive the ESU LAI of *L. principis-rupprechtii* forests.

2. Theory

2.1. Corrected Needle-to-Shoot Area Ratio and Canopy Element Clumping Index

The clumping effect of coniferous forest canopies is usually described at the two scales of within-shoots (needle-to-shoot area ratio) and beyond-shoots (Ω_e) [14,36]. The needle-to-shoot area ratio obtained from the shoot samples clipped from the canopy cannot be used directly in LAI estimation because the needle-to-shoot area ratio for woody components is equal to 1. Thus, the overestimation of the needle-to-shoot area ratio for woody components should be corrected in the PAI estimation using the method described in Zou et al. [14]. For the beyond-shoots clumping (Ω_e), several methods (e.g., DHP, DCP, MCI, and TRAC) and algorithms (e.g., gap size distribution (CC), logarithmic averaging (LX) [37], combination of gap size and logarithmic averaging (CLX) [32], modified logarithmic averaging [31], modified gap size distribution [33], and Pielou's coefficient of spatial segregation [38]) have been developed to estimate the Ω_e or Ω_w of leaf-on or leaf-off forests. The latter three Ω_e or Ω_w algorithms were not included in this study because Pielou's coefficient of spatial segregation algorithm tends to produce errors in the Ω_e or Ω_w estimates [19,31,35,38] and of the high similarities between CC and modified gap size distribution algorithms as well as LX and modified logarithmic averaging algorithms [19]. Zou et al. [19] reported that no universal Ω_e or Ω_w algorithm amongst CC, LX, and CLX outperforms others in deriving the Ω_e or Ω_w of leaf-on or leaf-off forests. Therefore, all three Ω_e or Ω_w algorithms of CC, LX, and CLX were used in this study. Table 1 lists the corrected needle-to-shoot area ratio and Ω_e estimation formulae used in this study [23]. In this study, the equations of the three Ω_w algorithms of CC, LX, and CLX to estimate the Ω_w of leaf-off forest canopies from DHP or MCI are the same as those for estimating the $\Omega_{e\_CC}(\theta)$, $\Omega_{e\_LX}(\theta)$, and $\Omega_{e\_CLX}(\theta)$ of leaf-on forest canopies, respectively (Equations (1)–(3). Similarly, the Equation for DCP to estimate the Ω_w of leaf-off forest canopies is the same as Equation (4) for estimating the Ω_e of leaf-on forest canopies.

Table 1. Ω_e and corrected needle-to-shoot area ratio (γ_c) estimation formulae used in this study. γ is the needle-to-shoot area ratio. $F_m(0,\theta)$ is the measured total canopy element gap fraction at θ, $F_{mr}(0,\theta)$ is the total canopy element gap fraction after removing the large gaps resulting from the non-random distribution of the canopy element [39,40], $p_e(\theta)$ is the canopy element gap fraction at θ, $\overline{p_e(\theta)}$ is the mean canopy element gap fraction of all segments at θ, $\overline{ln[p_e(\theta)]}$ is the mean logarithmic canopy element gap fraction for all segments at θ [37], n is the segment number, $p_{e\_k}(\theta)$ is the canopy element gap fraction of segment k and $\Omega_{e\_CC\_k}(\theta)$ is the Ω_e of segment k [32]. $\varnothing$ and f_f are the crown porosity and foliage cover, respectively [41]. A_n is half the total needle area in a shoot. $A_p(0°,0°)$, $A_p(45°,0°)$, and $A_p(90°,0°)$ are the shoot projection areas at azimuth angle 0° and zenith angles 0°, 45°, and 90°, respectively [42].

Equations		References
$\Omega_{e\_CC}(\theta) = \frac{ln(F_m(0,\theta))}{ln(F_{mr}(0,\theta))} * \left[1 + \frac{F_m(0,\theta) - F_{mr}(0,\theta)}{1 - F_m(0,\theta)}\right]$	(1)	[43]
$\Omega_{e\_LX}(\theta) = \frac{ln\left[\overline{p_e(\theta)}\right]}{\overline{ln[p_e(\theta)]}}$	(2)	[37]
$\Omega_{e\_CLX}(\theta) = \frac{nln\left[\overline{p_e(\theta)}\right]}{\sum_{k=1}^{n} ln[p_{e\_k}(\theta)]/\Omega_{e\_CC\_k}(\theta)}$	(3)	[32]
$\Omega_{e\_DCP}(0) = \frac{(1-\varnothing)\ln(1-f_f)}{\ln(\varnothing)/f_f}$	(4)	[41]
$\gamma = \frac{A_n}{\frac{A_p(0°,0°)*\cos(15°)+A_p(45°,0°)*\cos(45°)+A_p(90°,0°)*\cos(75°)}{\cos(15°)+\cos(45°)+\cos(75°)}}$	(5)	[42]
$\gamma_c = 1 * \frac{WAI}{PAI} + \gamma * [PAI - WAI]/PAI$	(6)	[14]

2.2. PAI, WAI, and LAI

The inversion model is a key factor that affects the PAI or LAI estimation from optical methods due to the large differences observed between the PAIs or LAIs obtained using different inversion models [19,23,24,35]. Two fundamental inversion models were proposed previously and are widely used in the ESU LAI estimation of forests, i.e., Beer's Law (Beer) (Equations (8) and (12)) [44] and Miller theorem (Miller) (Equations (9) and (13)) [45]. However, these two fundamental inversion models are unsuitable for all optical methods because the zenith angle ranges covered by these methods differ from those of the Miller theorem (0°–90°), such as LAI-2000/LAI-2200 (0°–74°) and DCP (0°–15°) methods. Therefore, several inversion models were proposed with the development of these optical methods [14,19,41,46]. For example, Equation (10) or (14) is the modified Miller integration adopted by the LAI-2200 method (LAI-2200) in estimating the PAI or LAI of forest canopies [23,46]. Similarly, Equation (11) is also the modified Miller integration adopted by the MCI method (MCI_0-85) for estimating the PAI of forest canopies [14,23]. Table 2 lists the inversion models used in the present study.

Table 2. The inversion model formulae used for the plant area index (PAI), wood area index (WAI), and leaf area index (LAI) estimations in this study. γ_c is the corrected needle-to-shoot area ratio. $G_e(\theta)$ is the canopy element projection coefficient (G_e) at θ. G_{e_i} is the G_e of the i^{th} annulus. $\Omega_e(\theta)$ is the Ω_e at θ derived from the gap size distribution (CC), logarithmic averaging (LX), and combination of gap size and logarithmic averaging (CLX) using Equations (1)–(3), respectively. $p_e(57)$ and $\Omega_e(57)$ are the canopy element gap fraction and Ω_e measurements obtained at the zenith angle range of 52°–62°, respectively. θ_i, $p_{e\_i}(\theta_i)$, Ω_{e_i}, and W_i are the center zenith angle, canopy element gap fraction, Ω_e and weight factor of the i^{th} annulus of digital hemispherical photography (DHP) or multispectral canopy imager (MCI), respectively. For the LAI-2200 method, the zenith angle ranges of the five annuli are 0°–13°, 16°–28°, 32°–43°, 47°–58°, and 61°–74°, respectively [19,46]. The W_i of the five annuli of LAI-2200 are 0.041, 0.131, 0.201, 0.29, and 0.337, respectively [19,46]. For MCI, the zenith angle ranges of the nine annuli are 0°–5°, 5°–15°, 15°–25°, 25°–35°, 35°–45°, 45°–55°, 55°–65°, 65°–75°, and 75°–85°, respectively (Equation (11)) [23]. The W_i of the nine annuli of MCI_0-85 are 0.0038, 0.0303, 0.0596, 0.0872, 0.1120, 0.1335, 0.1510, 0.1640, and 0.2580, respectively [23]. f_c is the crown cover. α is the woody-to-total area ratio. α_i is the α of the i^{th} annulus of MCI. α_{DCP} is obtained by averaging the α of the first and second annuli of MCI derived using CC.

Equations		References
$\text{PAI} = \frac{-ln(p_e(\theta))cos(\theta)\gamma_c}{G_e(\theta)\Omega_e(\theta)}$	(7)	[44]
$PAI_{Beer} = -2ln(p_e(57))cos(57)\gamma_c/\Omega_e(57)$	(8)	[19,44]
$PAI_{Miller} = -2\int_0^{\frac{\pi}{2}} \frac{\ln[p_e(\theta)]\gamma_c}{\Omega_e(\theta)} cos(\theta)sin(\theta)d\theta$	(9)	[45]
$PAI_{LAI-2200} = -\sum_{i=1}^{5} \frac{ln[p_{e\_i}(\theta_i)]\gamma_c cos(\theta_i)W_i}{G_{e\_i}\Omega_{e\_i}}$	(10)	[19,46]
$PAI_{MCI\_0-85} = -\sum_{i=1}^{9} \frac{ln[P_{e\_i}(\theta_i)]\gamma_c cos(\theta_i)W_i}{G_{e\_i}\Omega_{e\_i}}$	(11)	[23]
$LAI_{Beer} = -2ln(p_e(57))\cos(57)\gamma_c(1-\alpha_7)/\Omega_e(57)$	(12)	[19,44]
$LAI_{Miller} = -2\int_0^{\frac{\pi}{2}} \frac{\ln[p_e(\theta)]\gamma_c(1-\alpha)}{\Omega_e(\theta)} cos(\theta)sin(\theta)d\theta$	(13)	
$LAI_{LAI-2200} = -\sum_{i=1}^{5} \frac{ln[p_{e\_i}(\theta_i)]\gamma_c(1-\alpha)cos(\theta_i)W_i}{G_{e\_i}\Omega_{e\_i}}$	(14)	[19,46]
$LAI_{DCP} = -\frac{f_c ln(\varnothing)\gamma_c(1-\alpha_{DCP})}{G_e(0)/cos(0)}$	(15)	[41]

Zou et al. [19] reported that the impact of the assumption of spherical angle distribution of canopy element or woody components (canopy element or woody components projection coefficient is equal to be 0.5) on the ESU PAI and WAI estimations of the leaf-on and leaf-off forests from DHP can be reduced to a low level (<4%) if the three inversion models of Miller, LAI-2200 and Beer are adopted in the estimation. Therefore, that assumption was made in this study. The equations of the three inversion models (e.g., Beer, Miller, and LAI-2200) to estimate the WAI of the leaf-off forests from DHP are the same as those used for estimating the PAI of the leaf-on forests, respectively (Equations (8)–(10)). Similarly, the equations of the two inversion models (e.g., Beer and MCI_0-85) to estimate the WAI of the leaf-off forests from MCI are the same as those used for estimating the PAI of the leaf-on forests, respectively (Equations 8 and 11). For DCP, the equations used to estimate the PAI and WAI of the leaf-on and leaf-off plots are the same to derive LAI (Equation (15)) by assuming that the woody-to-total area ratio value is equal to zero. If the PAI and WAI measurements are simultaneously available, then the LAI of leaf-on forests also can be calculated as follows:

$$LAI = PAI - WAI \tag{16}$$

2.3. Woody-to-Total Area Ratio (α)

The α of leaf-on forests can be derived based on the WAI and PAI as follows [14]:

$$\alpha = {}^{WAI}/_{PAI} \tag{17}$$

If the WAI and PAI in Equation (17) are derived using Equation (7) based on the canopy element gap fraction ($p_{e\_i}(\theta_i)$), woody components gap fraction ($p_{w\_i}(\theta_i)$), Ω_{e_i}, and Ω_{w_i} of the i^{th} annulus of the MCI, respectively, then the estimate derived from Equation (17) is α_i.

3. Materials and Methods

3.1. Plot Description

Five forest plots with varying LAIs, stand densities, mean tree heights and tree ages (Table 3) were selected as the long-term observation ESUs with a size of 25 m × 25 m for validating LAI map products. The selected plots are located in the Saihanba National Forest Park in Hebei Province, China [23]. The dominant tree species in the park is *L. principis-rupprechtii*, which is a tree species that is spread widely in the northern area of China [47]. The five plots are single-species plots with the tree species of *L. principis-rupprechtii*, and the tree ages covered by the five even-aged plots are the typical tree ages of the park. The plots are at least 120–300 m away from the forest border with a flat terrain [47]. The canopy structure characteristics (e.g., tree height, diameter at breast height (DBH), tree age, stand density, and LAI) of the canopy around the plots are similar to those of the canopies of the plots [47]. Forest inventory was collected during the field campaign in 2017. Table 3 presents the site description of the five plots.

Table 3. Characteristics of the *L. principis-rupprechtii* plots [23].

	Plot 1	**Plot 2**	**Plot 3**	**Plot 4**	**Plot 5**
Longitude and latitude	42°24′43″ N, 117°19′4″ E	42°24′2″ N, 117°18′40″ E	42°18′2″ N, 117°18′9″ E	42°25′22″ N, 117°19′32″ E	42°17′42″ N, 117°16′53″ E
Mean tree height (m)	19.43	20.4	12.58	13.31	8.73
Average DBH (cm)	26.58	27.22	12.71	14.14	9.23
Mean element width (mm)	21.66	23.34	17.91	21.09	17.60
Stand density (stems/ha)	464	384	2320	1760	3904
Tree age (approximate years)	54	55	21	22	13
Corrected needle-to-shoot area ratio (γ_c)	1.30	1.17	1.14	1.17	1.28
Woody-to-total area ratio (α)	0.16	0.16	0.20	0.24	0.23
Litter collection LAI	4.65	3.58	4.96	3.04	6.69
Slope	~0°				
Tree species	*Larix principis-rupprechtii*				

3.2. Data Collection and Processing

3.2.1. TRAC

The TRAC measurements were collected in the five plots using TRAC-II (Nanjing Huiming Instrument Inc., Nanjing, China). The leaf-on TRAC measurements were collected between 11 August and 12 September 2017 at the maximum PAI (maximum LAI) of the plots [48–50]. The leaf-off TRAC measurements were collected between 30 October and 15 November 2017 at the minimum PAI (LAI = 0) of the plots. For the leaf-on plots, approximately six TRAC measurements were collected with the zenith angles within the maximum range of local solar elevation angle (0°–70°) with an interval of 10°. For the leaf-off plots, approximately four TRAC measurements were collected with the zenith angles within the maximum range of local solar elevation angle (0°–40°) with an interval of 10°. The TRAC instrument was operated at a height of approximately 1.2 m. The transect length of each TRAC measurement ranged from 100 m to 170 m and it was divided into several 10-m sub-transects using the flags. All TRAC measurements were collected under clear days. The TRAC measurements

were processed using TRACWin software (version 5.5.4). Some TRAC measurements were not correctly stored by the instrument because of the Bluetooth module failure. Thus, these measurements were not used in this study. The measurements with the photosynthetic photon flux density equal to zero were not used in this study because no gaps were detected by TRAC. Only the TRAC measurements with zenith angles near 57° were adopted to derive the ESU LAI of the five forests.

3.2.2. DCP

The DCP images were collected at a resolution of 5472 pixels × 3648 pixels using a Canon EOS 6D camera equipped with a Canon 24–70 mm lens. The focal length of the camera was fixed at 24 mm. The camera height was approximately 1.2 m. Manual mode was used to avoid overexposure and underexposure of the image collection. All images were collected under an overcast sky, before sunrise or after sunset. A sampling scheme with 16 sampling points that were evenly distributed within the plot with a 5-m distance was adopted for DCP image collection. The leaf-on DCP images were collected between 11 August and 3 September 2017 at the maximum PAI of the forests [48–50]. The leaf-off DCP measurements were collected between 30 October and 9 November 2017 at the minimum PAI of the forests. A total of 160 DCP images were obtained from the five forests. The center areas of the original DCP images were clipped into a new image with a resolution of 2227 pixels × 2061 pixels (a field of view of approximately 15° × 15°) before further processing. Then, the clipped images were processed using Adobe PhotoShop 7.0 (Adobe Inc., USA) following the procedures described by Macfarlane et al. [41]. Subsequently, the Ω_e and Ω_w of the five leaf-on and leaf-off forests for DCP were calculated using Equation (4) following the same procedures described by Macfarlane et al. [41], respectively. Two LAI estimates were obtained for each plot. One LAI estimate was derived using Equation (15) from the leaf-on DCP images. Another LAI estimate was obtained based on the derived PAI and WAI measurements using Equation (16). The PAI and WAI of leaf-on and leaf-off plots were obtained using Equation (15) by assuming that the woody-to-total area ratio value is equal to zero based on the leaf-on and leaf-off DCP images, respectively.

3.2.3. DHP

The sampling scheme of DHP was the same as that of DCP. DHP images were collected using a Canon 6D camera equipped with a Sigma 8 mm fisheye lens [23]. The DHP image resolution was 5472 pixels × 3648 pixels. The camera height was approximately 1.2 m. Manual mode was used to avoid overexposure and underexposure of the DHP image collection [23]. The DHP images were collected before sunrise, after sunset, or under overcast sky conditions. The leaf-on DHP images were collected between 11 August and 2 September 2017 at the maximum PAI of the five forests [48–50], whilst the leaf-off DHP images were collected between 30 October and 15 November 2017 at the minimum PAI of the five forests. A total of 160 DHP images were obtained from the five plots.

The procedures described in Gonsamo and Pellikka [51] were adopted to process the DHP images, including selecting the blue channel, applying a correction to the gamma and thresholding to classify the canopy element and sky. The classified images were then inputted into MTVSP (version 2018) [23,52] to calculate $p_e(\theta)$, $p_w(\theta)$, $\Omega_e(\theta)$, $\Omega_w(\theta)$, WAI, PAI, and LAI. The two segment sizes of 5° and 15° were selected for LX and CLX in the Ω_e or Ω_w estimations, respectively. The detailed explanation of the choice of the two segment sizes can be found in the work of Zou et al. [47].

Three $\Omega_e(\theta)$ or $\Omega_w(\theta)$ estimates were derived by using CC, LX, and CLX at each zenith angle in the zenith angle range of 10° to 90° with an interval of 1° in each forest (one estimate for each Ω_e or Ω_w algorithm). To obtain 91 $\Omega_e(\theta)$ and $\Omega_w(\theta)$ estimates that match the $p_e(\theta)$ and $p_w(\theta)$ measurements at the same zenith angle range of 0° to 90° with an interval of 1° in each forest, the $\Omega_e(\theta)$ or $\Omega_w(\theta)$ at the zenith angles ranging from 0° to 9° were assumed to be equal to $\Omega_e(10)$ or $\Omega_w(10)$ [19]. Two LAI groups (9 estimates of each group for the nine combinations of the three Ω_e algorithms and inversion models) were calculated for each forest using Equations (12)–(14) based on $p_e(\theta)$, $p_{e\_i}(\theta_i)$, $\Omega_e(\theta)$, Ω_{e_i}, corrected needle-to-shoot area ratio, and destructive or MCI woody-to-total

area ratio measurements. In addition to the LAI estimates derived using Equations (12)–(14) based on the leaf-on DHP images, another alternative to derive the ESU LAI of the five forests was based on the PAI and WAI estimates of the leaf-on and leaf-off forests, respectively. One PAI group (9 estimates for the nine combinations of the three Ω_e algorithms and inversion models) was calculated for each leaf-on forest using Equations (8)–(10) based on the $p_e(\theta)$, $p_{e\_i}(\theta_i)$, $\Omega_e(\theta)$, Ω_{e_i}, and corrected needle-to-shoot area ratio measurements. One group of WAI (9 estimates for the nine combinations of the three Ω_w algorithms and inversion models) was calculated for each leaf-off forest using Equations (8)–(10) based on the $p_w(\theta)$, $p_{w\_i}(\theta_i)$, $\Omega_w(\theta)$, and Ω_{w_i} measurements (corrected needle-to-shoot area ratio was assumed to be equal to 1). Then, another LAI group (9 estimates) could be derived using Equation (16) based on the two groups of PAI and WAI. Thus, 27 ESU LAI estimates were obtained for each forest.

3.2.4. MCI

The detailed procedures of collecting and processing MCI images can be found in the work of Zou et al. [23]. We provide a brief description here. Both leaf-on and leaf-off MCI images were collected from the same two representative sampling points in each forest. The MCI image pairs of each sampling point were collected in zenith directions ranging from 0° to 80° with an interval of 10° [23]. The MCI instrument height was approximately 1.2 m. Six azimuthal measurements were collected at each zenithal direction with an interval of 60° [14,23]. The MCI image resolution was 3488 pixels × 2616 pixels. The leaf-on and leaf-off MCI images of the five forests were collected at the same or similar period of the leaf-on and leaf-off DHP or DCP image collection, respectively. A total of 1080 MCI image pairs were collected from the five forests. The MCI image pairs were processed using ENVI 4.7 (Harris Geospatial Solutions Inc., USA) with the "IsoData" classification method [14]. The MCI image pairs were eventually classified into three classes of sky, woody components, and shoots, respectively [23]. The full size of each pixel of the MCI images was calculated based on the field of view of MCI, the image resolution, mean tree height of the plot and zenith angles where the images were collected [14,23]. Then, the pixel number in each segment which is required as the key parameter for LX and CLX to derive Ω_e or Ω_w can be obtained based on the derived values of the full size of each pixel. The classified MCI images were inputted into MTVSP (version 2018) [23,52] to calculate $p_e(\theta)$, $P_{e\_i}(\theta_i)$, $p_w(\theta)$, $P_{w\_i}(\theta_i)$, $\Omega_e(\theta)$, Ω_{e_i}, $\Omega_w(\theta)$, Ω_{w_i}, WAI, PAI, and LAI of each forest.

For MCI, both MCI_0-85 and Beer were used for the LAI estimation. The seventh annulus (55°–65°) of MCI was adopted by the Beer inversion model in the LAI estimation. One group of six PAI estimates (one estimate for each combination of the Ω_e algorithm and the inversion model) was calculated using Equations (8) and (11) based on the $p_{e\_i}(\theta_i)$, $p_e(57)$, Ω_{e_i}, and $\Omega_e(57)$, which were calculated from the classified leaf-on MCI images, and corrected needle-to-shoot area ratio measurements. Two groups of twelve WAI estimates (one estimate for each combination of the Ω_w algorithm and inversion model) were derived using Equations (8) and (11) based on the $p_{w\_i}(\theta_i)$, $p_w(57)$, Ω_{w_i}, and $\Omega_w(57)$ measurements that were calculated from the classified leaf-on and leaf-off MCI images, respectively. Then, 12 LAI estimates were derived from the MCI in each forest using Equation (16) based on the one PAI group and two WAI group measurements.

For MCI, only the MCI_0-85 inversion model was used for the woody-to-total area ratio determination of the five forests. The woody-to-total area ratio values of the five forests were calculated using Equation (17) based on the obtained PAI and WAI measurements, which were derived using Equation (11). Detailed procedures for obtaining the woody-to-total area ratio of the five forests from MCI can be found in Zou et al. [23].

3.2.5. Mean Element Width, Litter Collection LAI, Corrected Needle-to-Shoot Area Ratio and Woody-to-Total Area Ratio

The mean element width, litter collection LAI, corrected needle-to-shoot area ratio and destructive woody-to-total area ratio of the five plots were obtained during the field campaign. The detailed procedure of obtaining the mean element width, corrected needle-to-shoot area ratio, and destructive

woody-to-total area ratio measurements of the five plots can be found in the work of Zou et al. [23]. Here, we provide a brief description. The mean element width of each plot was obtained using typical shoot samples clipped from the three height classes of forest canopies (i.e., top, middle, and bottom) (two to four typical shoot samples for each height class). Then, the method described by Leblanc et al. [53] was used to calculate the mean element width of each typical shoot. The mean element width of each plot is the average of the mean element width values of all typical shoots of each plot [23]. Another group of 2-4 typical shoots was clipped from each height class of the canopy (i.e., top, middle, and bottom) for the needle-to-shoot area ratio calculation in each plot. The projection areas of each typical shoot were obtained using a Canon 6D camera equipped with a Canon 24–70 mm lens by rotating the shoot's main axis at azimuth angle 0° and zenith angles 0°, 45°, and 90°, respectively [23]. The half the total needle area of each typical shoot was obtained using the volume displacement method described by Chen et al. [36]. Then, the needle-to-shoot area ratio of each typical shoot was calculated using Equation (5) based on the three projection areas and half the total needle area measurement of the shoot. The needle-to-shoot area ratio of each plot was obtained by averaging the needle-to-shoot area ratio of all typical shoots of each plot [23]. Thereafter, the corrected needle-to-shoot area ratio of each plot was calculated using Equation (6) based on the needle-to-shoot area ratio and woody-to-total area ratio measurements.

The destructive method was used to measure the destructive woody-to-total area ratio values of five plots. Two or three representative trees were harvested in each plot. Then, the woody components (i.e., stem, branch, and fruit) area of each harvested tree was measured using a tape measure or digital caliper by assuming that the stem or branch sections were circular truncated cones and the fruits were spheroids [23]. The leaf area of each harvested tree was calculated using the dry mass of all needles and the specific leaf area of the harvested tree. The specific leaf area of the harvested tree was determined based on the dry mass and the hemisurface area of a number of typical needles (approximately 300–350) which was estimated using the volume displacement method [36]. Afterward, the woody-to-total area ratio value of each harvested tree was calculated based on the woody components area and needle areas of all needles of each tree. Finally, the destructive woody-to-total area ratio value of each plot was obtained based on the woody-to-total area ratio values of the harvested trees and the DBH measurements of all trees of the plot [23].

The litter collection LAI of the five plots was obtained using the litter collection measurements. Nine litter traps with a size of 50 cm × 50 cm were evenly placed in each plot with a distance of 6.25 m. The trap height was approximately 0.5 m. Six litter collection measurements were collected from 1 September 2017 to 28 October 2017 with a time interval of approximately one to two weeks [47]. The specific leaf area of the collected typical needles was derived using the same method applied in the woody-to-total area ratio estimation of the representative trees. Then, the litter collection LAI of each plot was obtained based on the specific leaf area and dry mass of all collected needles. Details of the determination of litter collection LAI for each plot can be found in the work of Zou at al. [47].

4. Results

4.1. Gap Fraction

Large differences were observed between the $p_e(\theta)$ or $p_w(\theta)$ of the four optical methods in the five plots (Figures 1 and 2). For example, the difference between the $p_w(0)$ of DHP and MCI was as large as 0.45 in leaf-off plot 5 (Figure 2). However, no large differences were observed between the $p_e(\theta)$ or $p_w(\theta)$ of TRAC and MCI even though the estimates of TRAC tended to be slightly smaller than those of MCI in most cases (Figures 1 and 2). We also found that the $p_e(\theta)$ or $p_w(\theta)$ of MCI was smaller than those of DHP and DCP in the five leaf-on or leaf-off plots (Figures 1 and 2). Similarly, the $p_e(0)$ or $p_w(0)$ of DHP tended to be larger than those of DCP in most cases (Figures 1 and 2). The differences between the $p_e(\theta)$ or $p_w(\theta)$ of the four optical methods tended to decrease with the increasing zenith angles due to the $p_e(\theta)$ or $p_w(\theta)$ estimates of the four methods were decreased with zenith angles obviously.

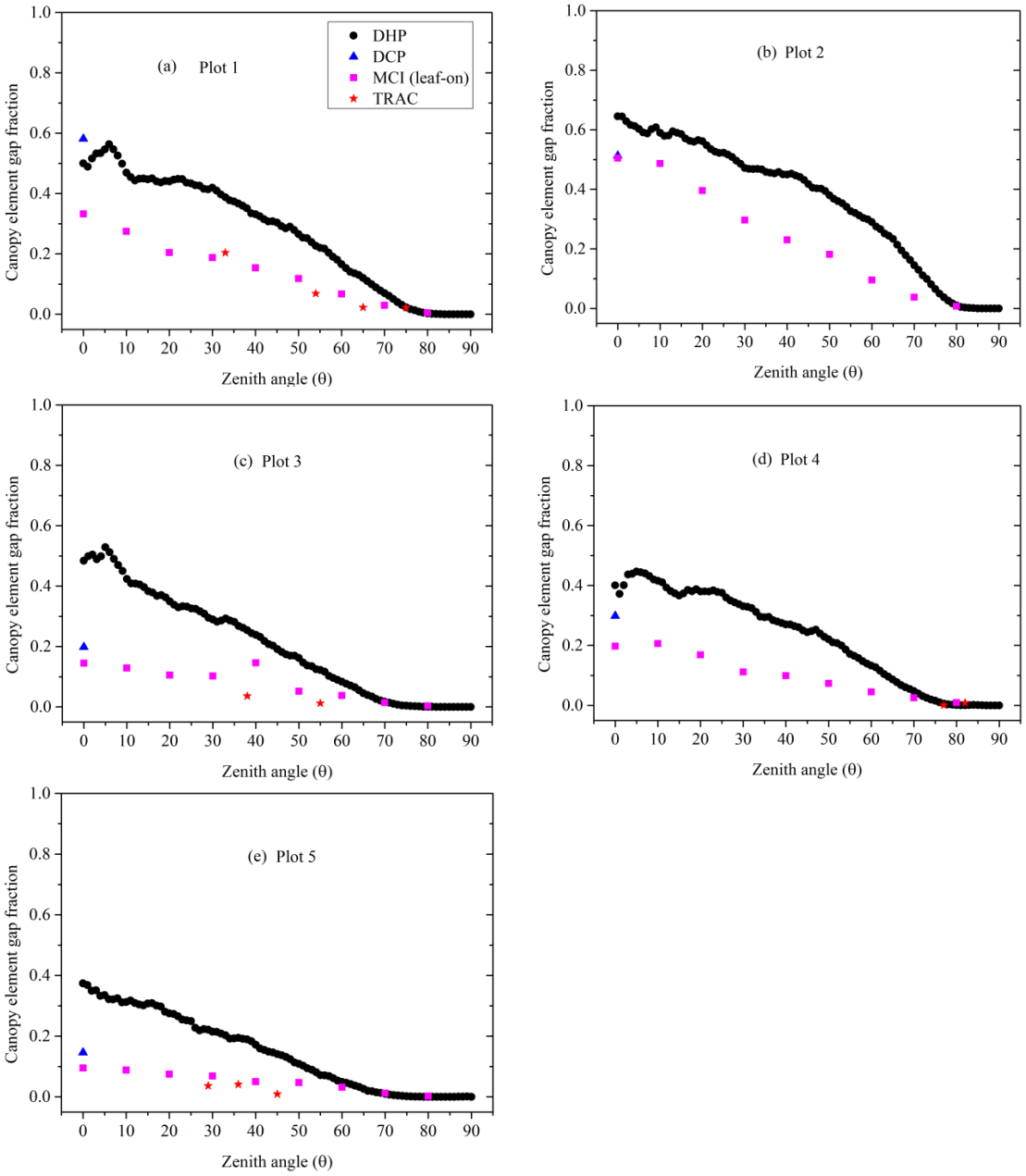

Figure 1. Canopy element gap fraction ($p_e(\theta)$) measurements obtained from DHP, tracing radiation of canopy and architecture (TRAC), MCI, and digital cover photography (DCP) in the five leaf-on plots: (**a**) plot 1, (**b**) plot 2, (**c**) plot 3, (**d**) plot 4, and (**e**) plot 5.

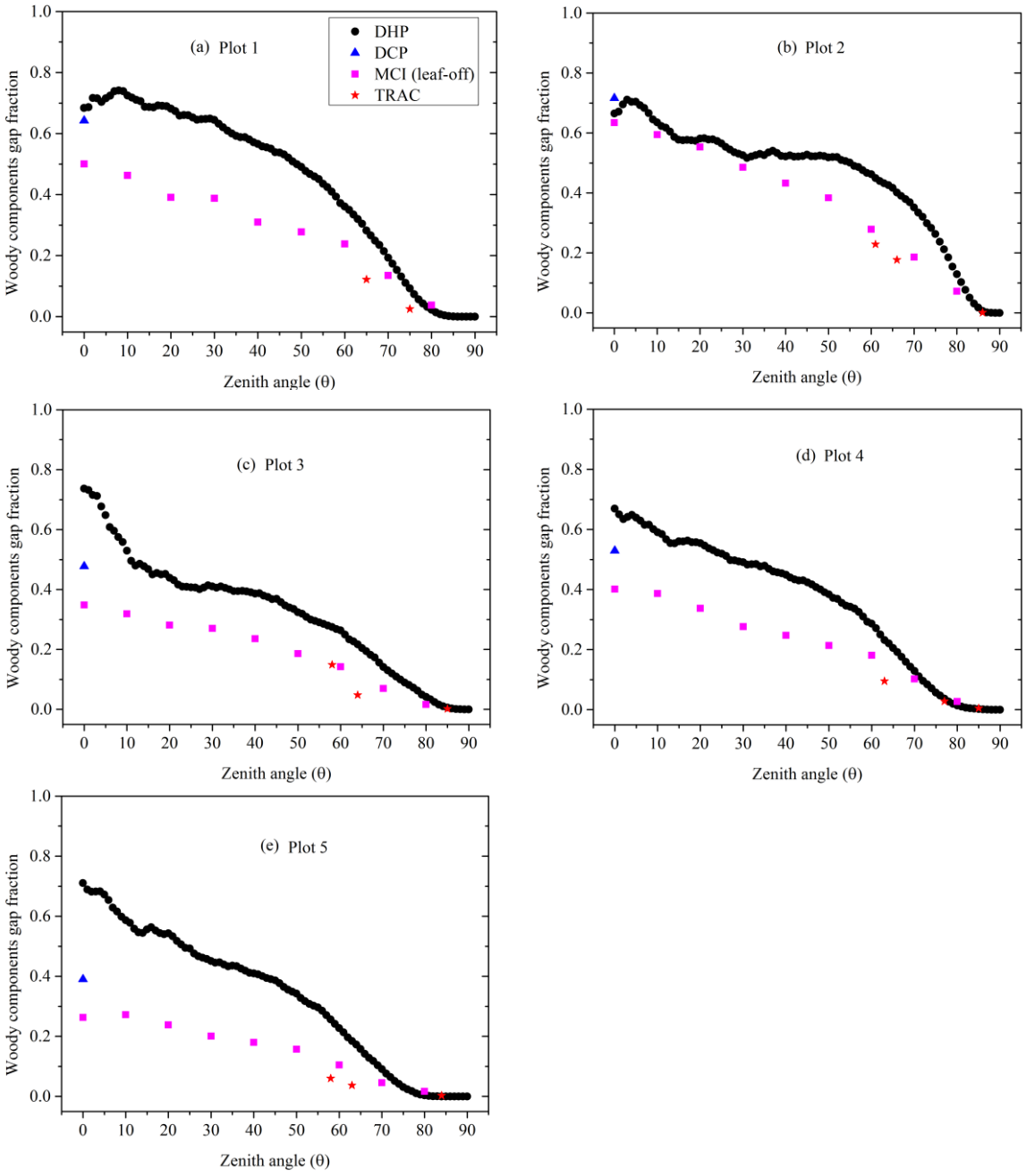

Figure 2. Woody components gap fraction ($p_w(\theta)$) measurements obtained from DHP, TRAC, MCI, and DCP in the five leaf-off plots: (**a**) plot 1, (**b**) plot 2, (**c**) plot 3, (**d**) plot 4, and (**e**) plot 5.

4.2. Canopy Element and Woody Components Clumping Indices

Large differences were observed between the $\Omega_e(\theta)$ or $\Omega_w(\theta)$ obtained from DHP and MCI using the same Ω_e or Ω_w algorithm as well as from DHP or MCI using different Ω_e or Ω_w algorithms in the five leaf-on or -off plots (Figures 3 and 4). For example, the differences between the $\Omega_e(60)$ of DHP and MCI in leaf-on plot 2 are 0.25, 0.16, and 0.05 for the three Ω_e algorithms of CC, LX, and CLX, respectively (Figure 3); the differences between the $\Omega_e(60)$ of CC and LX as well as CC and CLX in leaf-on plot 2 are 0.36 and 0.47 for DHP, respectively (Figure 3). However, the trend of the $\Omega_e(\theta)$ or $\Omega_w(\theta)$ obtained from TRAC was nearer to that of MCI derived using CC with a similar zenith angle in the five leaf-on or leaf-off plots, except leaf-on plot 5 in most circumstances (Figures 3 and 4). Similarly, no large differences were found between the $\Omega_e(0)$ or $\Omega_w(0)$ measurements obtained from DCP and MCI using CC in the five leaf-on plots, except plots 1, 2, and 5, or five leaf-off plots, except plots 1 and 2

(Figures 3 and 4). Interestingly, no large differences (<0.07) were observed between the $\Omega_e(\theta)$ or $\Omega_w(\theta)$ obtained from MCI using LX and CLX in the five leaf-on or leaf-off plots, except leaf-off plot 5 (Figures 3 and 4). For DHP, CC tended to produce $\Omega_e(\theta)$ or $\Omega_w(\theta)$ estimates equal to 1 at the zenith angle range of approximately 40°–90° in the five leaf-on or leaf-off plots (Figures 3 and 4). That indicates that CC was not performed well in estimating the Ω_e or Ω_w of the five leaf-on or leaf-off plots from DHP at the zenith angle range of 40°–90°.

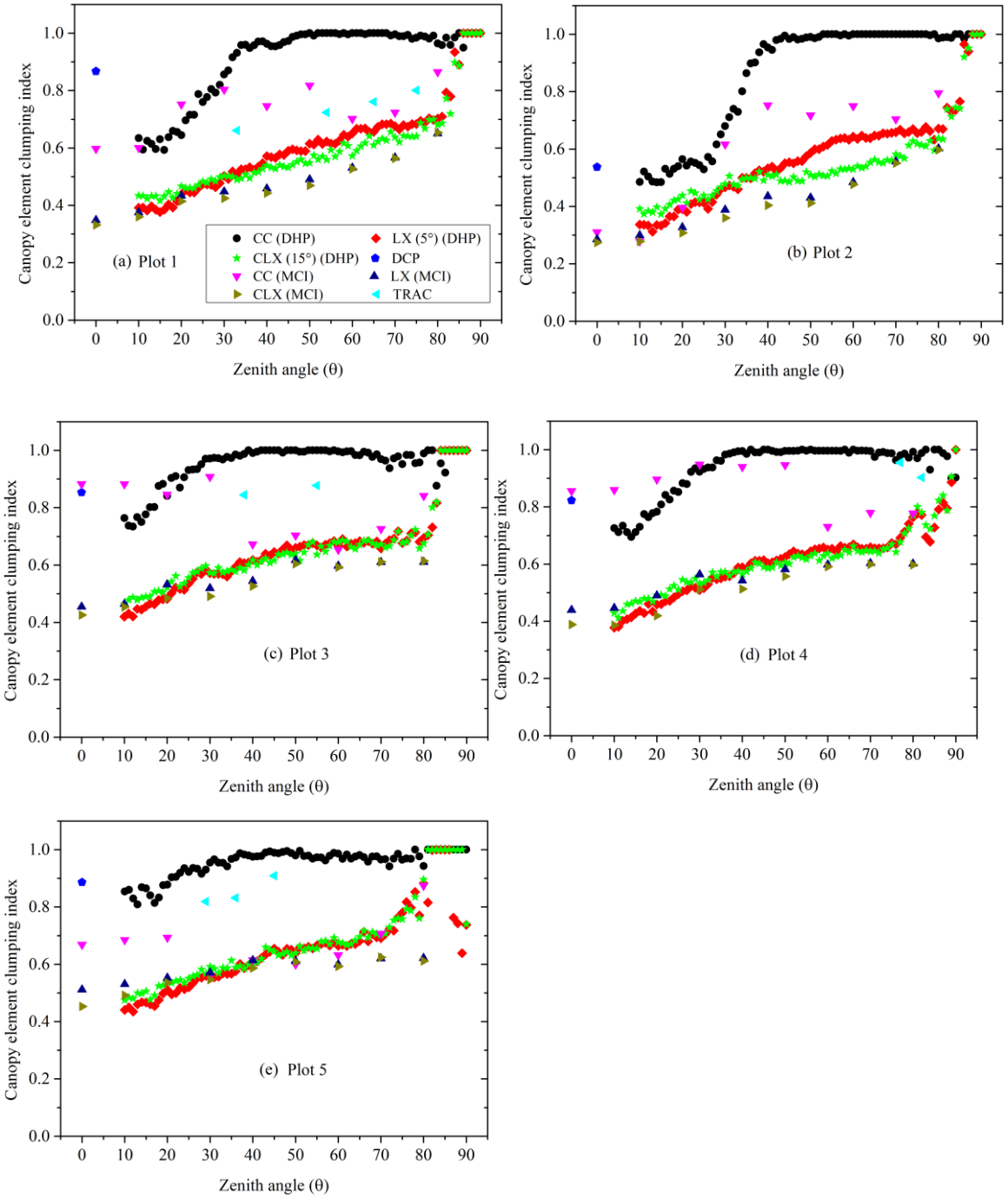

Figure 3. Canopy element clumping index ($\Omega_e(\theta)$) measurements obtained from DHP, TRAC, MCI, and DCP in the five leaf-on plots: (**a**) plot 1, (**b**) plot 2, (**c**) plot 3, (**d**) plot 4, and (**e**) plot 5.

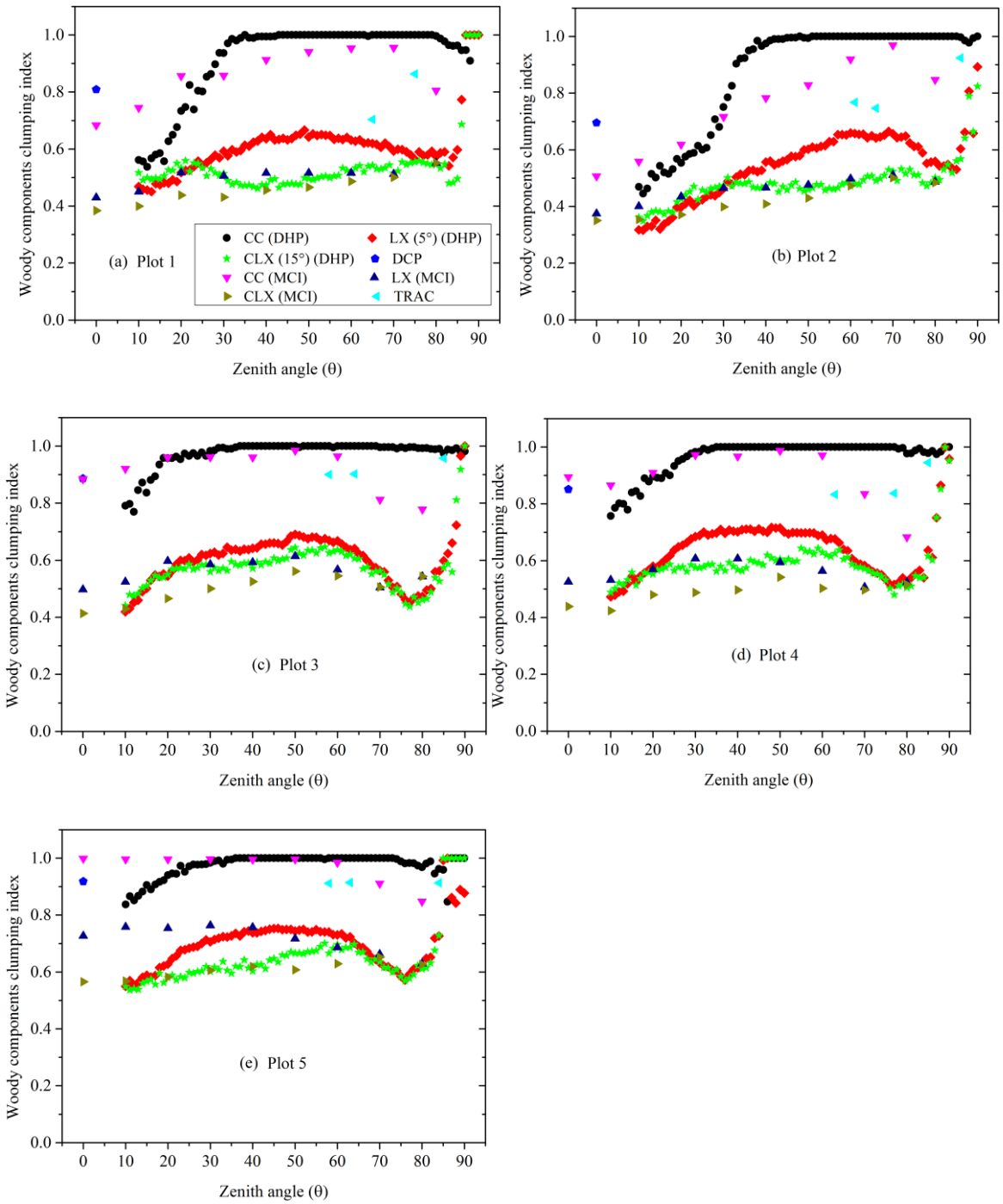

Figure 4. Woody components clumping index ($\Omega_w(\theta)$) measurements obtained from DHP, TRAC, MCI, and DCP in the five leaf-off plots: (**a**) plot 1, (**b**) plot 2, (**c**) plot 3, (**d**) plot 4, and (**e**) plot 5.

4.3. LAI

4.3.1. Canopy Element and Woody Components Clumping Index Algorithms

Tables 4–6 show that the LAI estimations of DHP and MCI were greatly affected by the Ω_e or Ω_w algorithm adopted in the estimation. Large differences were observed between the LAIs obtained from DHP or MCI using the same inversion model and woody components correction method but with different Ω_e or Ω_w algorithms in the five plots (Tables 4 and 6). For example, the differences in the LAIs obtained from DHP using the same inversion model and the woody components correction method but

with CC and LX or CC and CLX ranged from 0.73 to 1.54 (25%–47%) when destructive woody-to-total area ratio measurements were adopted in the estimation (Table 4). The differences between the RMSE and MAE of the LAI obtained from DHP using the same inversion model but with CC and LX or CC and CLX ranged from 0.94–1.17 (21%–25%) and 1–1.22 (23%–28%) when destructive woody-to-total area ratio measurements were used in the estimation (Table 5). By contrast, small differences were observed between the RMSE (0.01–0.24, 0%–5%) and MAE (0.03–0.23, 1%–5%) of the LAI obtained from DHP using the same inversion model and woody components correction method but with LX and CLX (Table 5). A similar trend of differences between the LAI obtained using the same inversion model and woody components correction method but with different Ω_e or Ω_w algorithms for DHP was also observed for MCI (Tables 6 and 7).

For DHP, CC tended to underestimate the ESU LAI of the five forests obviously compared with LX and CLX (Tables 4 and 5). LX and CLX outperformed CC in ESU LAI estimation with smaller RMSE and MAE for DHP regardless of the inversion model and woody components correction methods used in the estimation (Tables 4 and 5). Compared with DHP, CC outperformed LX and CLX in the ESU LAI estimation with the smallest MAE for MCI when the leaf-on MCI images were used in the estimation (Table 7).

Table 4. LAI derived from the leaf-on DHP images using the three canopy element or woody components clumping index (Ω_e and Ω_w) algorithms, three inversion models and destructive or MCI woody-to-total area ratio (α) or WAI obtained from the leaf-off DHP images in the five plots.

		Destructive α					**MCI α**					**WAI Obtained from Leaf-off DHP Images**				
Inversion Model	**Ω_e or Ω_w Algorithm**	**Plot 1**	**Plot 2**	**Plot 3**	**Plot 4**	**Plot 5**	**Plot 1**	**Plot 2**	**Plot 3**	**Plot 4**	**Plot 5**	**Plot 1**	**Plot 2**	**Plot 3**	**Plot 4**	**Plot 5**
Beer	CC	1.93	1.25	2.26	1.80	3.00	2.07	1.25	2.28	1.82	3.24	1.31	0.69	1.42	1.1	2.45
	LX	3.04	1.98	3.34	2.77	4.40	3.11	1.98	3.05	2.59	4.40	2.07	1.11	2.09	1.82	3.75
	CLX	3.30	2.38	3.37	2.86	4.38	3.34	2.35	2.95	2.52	4.10	2.01	1.15	1.99	1.74	3.55
Miller	CC	2.62	1.82	2.99	1.88	3.16	2.81	1.82	3.02	1.91	3.41	1.42	1.25	2.25	1.22	2.47
	LX	3.64	2.55	4.01	2.86	4.40	3.72	2.55	3.66	2.67	4.40	2.04	1.54	2.67	1.79	3.45
	CLX	3.75	2.69	4.01	2.85	4.32	3.79	2.66	3.51	2.51	4.04	1.92	1.52	2.56	1.62	3.21
LAI-2200	CC	1.99	1.41	2.18	1.83	2.87	2.14	1.41	2.21	1.85	3.09	1.38	0.68	1.29	1.12	2.29
	LX	3.19	2.22	3.37	2.96	4.41	3.27	2.22	3.07	2.77	4.41	2.25	1.04	2.28	1.95	3.68
	CLX	3.32	2.39	3.37	2.96	4.33	3.36	2.36	2.95	2.61	4.05	2.13	1.01	1.79	1.75	3.4

Table 5. Correlation statistics between the litter collection LAI and the LAI derived from the leaf-on DHP images using the three canopy element or woody components clumping index (Ω_e or Ω_w) algorithms, three inversion models, and destructive or MCI woody-to-total area ratio (α) or WAI obtained from the leaf-off DHP images in the five plots (two-tailed Student's *t*-test with 95% confidence level). The root mean square error (RMSE) and mean absolute error (MAE) are expressed in LAI units (m^2/m^2).

		Destructive α						**MCI α**						**WAI Obtained from Leaf-off DHP Images**					
Inversion Model	**Ω_e or Ω_w Algorithm**	**RMSE (%)**	**MAE (%)**	**R^2**	**Intercept**	**Slope**	***p***	**RMSE (%)**	**MAE (%)**	**R^2**	**Intercept**	**Slope**	***p***	**RMSE (%)**	**MAE (%)**	**R^2**	**Intercept**	**Slope**	***p***
Beer	CC	2.66 (58%)	2.54 (55%)	0.90	0.17	0.41	0.04	2.56 (56%)	2.45 (53%)	0.91	−0.03	0.47	0.03	3.28 (72%)	3.19 (70%)	0.92	−0.55	0.42	0.03
	LX	1.62 (35%)	1.48 (31%)	0.89	0.54	0.56	0.04	1.67 (37%)	1.56 (33%)	0.92	0.36	0.58	0.03	2.50 (54%)	2.42 (53%)	0.89	−0.63	0.61	0.04
	CLX	1.49 (33%)	1.33 (27%)	0.93	1.01	0.49	0.02	1.69 (37%)	1.53 (32%)	0.94	0.92	0.47	0.02	2.58 (56%)	2.50 (55%)	0.9	−0.51	0.57	0.04
Miller	CC	2.23 (49%)	2.09 (45%)	0.92	0.64	0.40	0.03	2.11 (46%)	1.99 (43%)	0.94	0.45	0.47	0.02	2.98 (65%)	2.86 (62%)	0.9	−0.01	0.38	0.04
	LX	1.29 (28%)	1.09 (22%)	0.92	1.17	0.51	0.03	1.34 (29%)	1.18 (24%)	0.96	0.98	0.53	0.01	2.38 (52%)	2.29 (50%)	0.94	−0.06	0.51	0.02
	CLX	1.28 (28%)	1.06 (21%)	0.92	1.37	0.47	0.03	1.48 (32%)	1.28 (26%)	0.92	1.27	0.44	0.03	2.51 (55%)	2.42 (53%)	0.95	−0.03	0.48	0.01
LAI-2200	CC	2.67 (58%)	2.53 (54%)	0.91	0.47	0.35	0.03	2.57 (56%)	2.44 (53%)	0.92	0.3	0.4	0.03	3.33 (73%)	3.23 (71%)	0.9	−0.37	0.38	0.04
	LX	1.53 (33%)	1.35 (28%)	0.89	0.95	0.50	0.04	1.59 (35%)	1.44 (30%)	0.91	0.76	0.52	0.03	2.43 (53%)	2.34 (51%)	0.88	−0.46	0.59	0.05
	CLX	1.50 (33%)	1.31 (26%)	0.91	1.18	0.46	0.03	1.69 (37%)	1.52 (31%)	0.92	1.08	0.43	0.03	2.67 (58%)	2.57 (56%)	0.86	−0.43	0.53	0.06

Table 6. LAI derived using the three canopy element or woody components clumping index (Ω_e or Ω_w) algorithms and inversion models from the leaf-on MCI images or both the leaf-on and leaf-off MCI images in the five plots. When only the leaf-on MCI images were used in the LAI estimation, the WAIs of the five plots were obtained using Equations (8) and (11) based on the leaf-on MCI images. When both the leaf-on and leaf-off MCI images were used in the LAI estimation, the WAIs of the five plots were obtained using Equations (8) and (11) based on the leaf-off MCI images. Then, the LAI of the five plots was derived using Equation (16) based on the PAI and WAI measurements.

		Leaf-on MCI Images					Leaf-on and Leaf-off MCI Images				
Inversion Model	**Ω_e or Ω_w Algorithm**	**Plot 1**	**Plot 2**	**Plot 3**	**Plot 4**	**Plot 5**	**Plot 1**	**Plot 2**	**Plot 3**	**Plot 4**	**Plot 5**
Beer	CC	4.92	3.53	5.21	4.41	6.47	3.80	2.48	4.02	3.50	5.11
	LX	6.12	5.28	4.94	4.79	6.23	4.17	3.38	3.07	3.31	4.45
	CLX	6.09	5.30	4.74	4.58	6.01	4.03	3.34	2.98	2.99	4.20
MCI_0-85	CC	3.77	3.10	3.71	2.94	5.63	2.57	2.15	2.50	1.89	4.40
	LX	5.40	4.28	4.40	4.04	5.57	3.48	2.70	2.65	2.66	4.17
	CLX	5.48	4.40	4.33	4.08	5.34	3.41	2.71	2.52	2.61	3.84

Table 7. Correlation statistics between the litter collection LAI and LAI derived from the leaf-on or both the leaf-on and leaf-off MCI images using the three canopy element or woody components clumping index (Ω_e or Ω_w) algorithms and the inversion models in the five plots (two-tailed Student's *t*-test with 95% confidence level). The RMSE and MAE are expressed in LAI units (m^2/m^2).

		Leaf-on MCI Images						Leaf-on and Leaf-off MCI Images					
Inversion Model	**Ω_e or Ω_w Algorithm**	**RMSE (%)**	**MAE (%)**	**R^2**	**Intercept**	**Slope**	***p***	**RMSE (%)**	**MAE (%)**	**R^2**	**Intercept**	**Slope**	***p***
Beer	CC	0.64 (14%)	0.43 (12%)	0.91	1.71	0.70	0.03	1.05 (23%)	0.99 (21%)	0.86	1.12	0.58	0.06
	LX	1.29 (28%)	1.08 (29%)	0.71	3.93	0.34	0.18	1.34 (29%)	1.02 (19%)	0.68	2.36	0.29	0.21
	CLX	1.26 (27%)	1.12 (29%)	0.62	3.94	0.31	0.26	1.45 (32%)	1.08 (20%)	0.70	2.21	0.28	0.19
MCI_0-85	CC	0.86 (19%)	0.75 (15%)	0.97	0.47	0.73	0.01	1.95 (43%)	1.88 (41%)	0.95	−0.34	0.66	0.01
	LX	0.85 (19%)	0.83 (19%)	0.81	2.89	0.40	0.09	1.67 (36%)	1.45 (29%)	0.83	1.30	0.40	0.08
	CLX	0.97 (21%)	0.93 (22%)	0.70	3.28	0.32	0.19	1.82 (40%)	1.57 (31%)	0.77	1.58	0.31	0.13

4.3.2. Inversion Model

Large differences were observed between the LAIs obtained from DHP using the same Ω_e or Ω_w algorithm and woody components correction method but with different inversion models in the five plots (Table 4). For example, the difference between the LAI of Miller and LAI-2200 for DHP was as large as 0.81 (27%) in plot 3 when CC and MCI woody-to-total area ratio were adopted in the estimation (Table 4). The differences between the RMSE and MAE of the LAI obtained from DHP using the same Ω_e algorithm and woody components correction method but with different inversion models were in the range of 0.0–0.45 (0%–10%) and 0.01–0.46 (0%–10%), respectively (Table 5). The LAI of Miller tended to be larger than LAI-2200 or Beer for DHP in the five plots in most cases (Table 4). Miller is amongst the three inversion models to derive the LAI with the smallest MAE and RMSE for DHP (Table 5).

Similar to DHP, a large difference (1.61, 46%) was also observed for MCI between the LAI of Beer and MCI_0-85 in plot 4 when CC and the WAI obtained from the leaf-off MCI images were adopted in the estimation (Table 6). The differences between the RMSE and MAE of the LAI obtained from MCI using the same Ω_e or Ω_w algorithm and woody components correction method but with different inversion models were in the range of 0.22–0.90 (5%–20%) and 0.19–0.89 (3%–20%) (Table 7). For MCI, the best inversion model for estimating the ESU LAI of the five forests changed with the Ω_e or Ω_w algorithm and woody components correction method adopted in the estimation (Table 7).

4.3.3. Woody Component Correction Method

The LAIs obtained from DCP, DHP, and MCI in the five plots were remarkably affected by the woody components correction methods used in the estimation (Tables 4–9). For example, the difference was as large as 1.87 (49%) in plot 1 between the LAIs obtained from the leaf-on DHP images using CLX and Miller but with two woody components correction methods of MCI woody-to-total area ratio and the WAI obtained from the leaf-off DHP images, respectively (Table 4). For DHP, large differences were observed between the RMSE or MAE of the LAIs obtained using the same Ω_e or Ω_w algorithm and inversion model but with two woody components correction methods of MCI woody-to-total area ratio and the WAI derived from the leaf-off DHP images in the range of 0.72–1.04 (16%–23%) or 0.74–1.14 (17%–27%) (Table 5). However, small differences were found for DHP between the RMSE or MAE of the LAIs obtained using the same Ω_e or Ω_w algorithm and inversion model but with MCI and destructive woody-to-total area ratio values (Table 5). Like DHP, large differences were also observed for MCI between the RMSE or MAE of the LAIs obtained using the same Ω_e or Ω_w algorithm and inversion model but with the two woody components correction methods, ranging from 0.05–1.09 (1%–24%) or 0.04–1.13 (9%–26%) (Table 7). The LAI obtained from DHP or MCI or DCP using the woody components correction method of WAI derived from the leaf-off DHP or MCI or DCP images was obviously smaller than that derived using the same inversion model and Ω_e or Ω_w algorithm but with other woody components correction methods (Tables 4, 6, and 8).

Table 8. LAI derived from DCP using two calculation schemes. One scheme calculates the LAI from the leaf-on DCP images (Equation (15)), and the other scheme calculates the LAI based on the PAI and WAI derived from the leaf-on and leaf-off DCP images, respectively (Equation (16)).

	Plot 1	Plot 2	Plot 3	Plot 4	Plot 5
Leaf-on DCP images	1.44	2.35	3.89	2.81	4.92
Leaf-on and leaf-off DCP images	0.53	1.94	2.66	1.95	3.5

Table 9. Correlation statistics between litter collection LAI and LAI derived from DCP using two calculation schemes (two-tailed Student's *t*-test with 95% confidence level). The RMSE and MAE are expressed in LAI units (m^2/m^2).

	RMSE (%)	MAE (%)	R^2	Intercept	Slope	*p*
Leaf-on DCP images	1.80 (39%)	1.50 (32%)	0.68	0.08	0.65	0.20
Leaf-on and leaf-off DCP images	2.70 (59%)	2.47 (53%)	0.56	0.13	0.43	0.33

4.3.4. LAI Estimation Methods

Tables 4, 6, 8, and 10 indicate large differences between the LAI obtained using the same or similar inversion models, Ω_e or Ω_w algorithm and woody components correction method but with different optical methods in the five plots. For example, the difference between the LAI of DCP derived from the leaf-on DCP images and that of MCI obtained from the leaf-on MCI images using CC and Beer is 3.48 (71%) in plot 1 (Tables 6 and 8). Amongst the four optical methods, TRAC exhibited the best performance in terms of obtaining the ESU LAI of the five forests with the smallest RMSE (0.31, 6%) and MAE (0.24, 4%) followed by MCI (Tables 5, 7, 9 and Figure 5). For MCI, the ESU LAIs with the smallest RMSE (0.64, 14%) and MAE (0.43, 12%) were obtained from leaf-on MCI images using CC and Beer (Table 7). DHP tended to underestimate the ESU LAI of the five forests regardless of the inversion model, Ω_e or Ω_w algorithm and woody components correction method used in the estimation (Tables 4 and 5). For DHP, the ESU LAIs with the smallest RMSE (1.28; 28%) and MAE (1.06; 21%) were obtained using Miller, CLX and destructive woody-to-total area ratio (Table 5). The trend of LAI underestimation for DHP in the five plots was also observed for DCP (Tables 8 and 9). MCI and TRAC did not systematically underestimate the LAI in the five plots (Tables 6 and 10). For plot 5 with a high litter collection LAI of 6.69, DHP, DCP, and MCI tended to underestimate the LAI (Tables 4, 6, and 8).

Table 10. LAIs derived using the leaf-on TRAC measurements and destructive woody-to-total area ratio values in the five plots. Only those TRAC measurements collected with a zenith angle near 57° were used for LAI estimation.

	Plot 1		Plot 3	Plot 5
θ	54.1°	64.85°	55.25°	44.9°
LAI	4.73	4.60	5.24	7.23

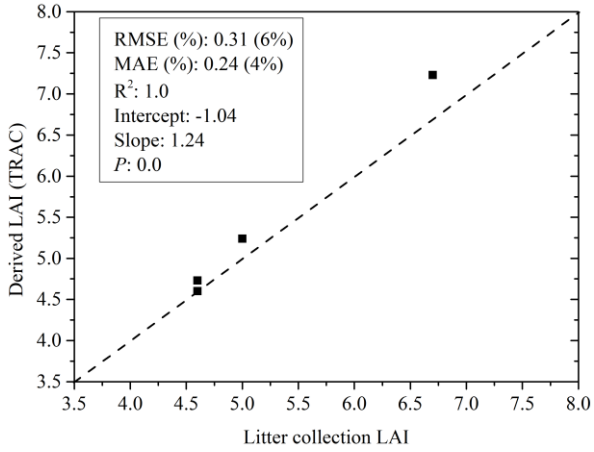

Figure 5. Comparison of LAI obtained from TRAC with litter collection LAI in the five plots. Statistics are given at 95% confidence level from the two-tailed Student's *t*-test. The RMSE and MAE are expressed in LAI units (m^2/m^2).

5. Discussion

5.1. Which Canopy Element or Woody Component Clumping Index Algorithm(s) or Inversion Model(s) Is (Are) More Reliable to Be Adopted in the ESU LAI Estimation of L. principis-rupprechtii Forests from DHP and MCI?

Based on Tables 4–7, the ESU LAI estimation of DHP and MCI was largely affected by the canopy element or woody components clumping index (Ω_e or Ω_w) algorithm and inversion model adopted in the estimation. This finding is consistent with the conclusions drawn in previous studies [19,24,32,41]. As expected, large differences were found between the LAIs obtained from DHP or MCI using the same inversion model and woody components correction method but with different Ω_e or Ω_w algorithms or the same Ω_e or Ω_w algorithm and woody components correction method but with different inversion models (Tables 4 and 6). Three factors contributed to the large LAI differences: the obvious variation of $p_e(\theta)$ or $p_w(\theta)$ and $\Omega_e(\theta)$ or $\Omega_w(\theta)$ at the zenith angle range of 0°–90° (Figures 1–4); the large differences between the $\Omega_e(\theta)$ or $\Omega_w(\theta)$ derived using different algorithms (Figures 3 and 4) and the different zenith angle ranges covered by the four inversion models (Table 2).

The best Ω_e or Ω_w algorithm for estimating the ESU LAI of the five forests changed with the optical methods. For DHP, CLX, and LX outperformed CC in obtaining LAIs with the smallest RMSE and MAE (Table 5). This finding is consistent with the finding of previous studies which reported that CLX and LX outperformed CC for DHP in estimating the Ω_e or Ω_w of the leaf-on or leaf-off forest plots [19,33,41]. For MCI, CC outperformed LX and CLX in LAI estimation with the smallest RMSE and MAE (Table 7). The different conclusions on the best Ω_e or Ω_w algorithm for DHP and MCI can be attributed to the following reasons: (1) DHP has the disadvantage of insufficient sampling at the zenith and a coarse resolution of DHP images at large zenith angles [54]. By contrast, MCI has the advantage of sampling the canopy with high resolution at all zenith angles. (2). The "P" method described by Chen and Cihlar [40], which was adopted by DHP to derive the mean element width values, tended to overestimate the mean element width values and result in Ω_e or Ω_w overestimation for CC. The good performance of CC in the ESU LAI estimation for MCI was further confirmed by the small RMSE and MAE of the LAI obtained from TRAC (Figure 5). This point illustrates that when the

canopy was sufficiently sampled and an accurate mean element width value was obtained, CC could provide relatively more accurate Ω_e or Ω_w estimates than those of LX and CLX. CC has two advantages in deriving Ω_e or Ω_w over LX and CLX. Firstly, CC requires no spatial distribution assumption of canopy element. By contrast, an assumption of the randomly distribution of canopy element at the segment scale with a length that is 10 times mean element width value was made for LX or CLX [37]. This assumption seems to almost hold true for MCI based on the close agreement between the Ω_e or Ω_w obtained from LX and CLX in most cases (Figures 3 and 4). The agreement illustrates that the canopy element at the segment scale approached random distribution. However, a reasonable guideline for defining the segment lengths of LX and CLX for DHP was unavailable. Obvious differences were found between the Ω_e or Ω_w of LX or CLX obtained with varying segment sizes [33,54]. Secondly, the large between-crown gaps, which dominated the clumping effects of forest canopies [39,40], can be effectively captured by CC, whereas LX or CLX was not qualified to detect and utilize such kinds of large gaps to derive Ω_e or Ω_w due to the small segment size.

The best inversion model for estimating the ESU LAI of the five forests was different between DHP and MCI (Tables 4–7). For DHP, Miller outperformed Beer and LAI-2200 in the ESU LAI estimation with the smallest RMSE and MAE (Table 5). For MCI, Beer outperformed MCI_0-85 in the LAI estimation with the smallest RMSE and MAE when CC was used in the estimation; by contrast, MCI_0-85 outperformed Beer in the LAI estimation when LX or CLX was adopted in the estimation (Table 7). This finding is consistent with the finding of Zou et al. [19] who reported that the best inversion model for estimating the PAI and WAI of leaf-on and leaf-off forest plots from optical methods is the function of the Ω_e or Ω_w estimation algorithm, PAI, LAI and WAI and the plant functional types of forests. When CC was adopted in the ESU LAI estimation, the best inversion model was expected with differences between DHP and MCI as the contrasting performance of CC in estimating the Ω_e or Ω_w of the five forests for DHP and MCI (Figures 3 and 4).

5.2. Which Woody Components Correction Method(s) Is (Are) Better in ESU LAI Estimation for the Four Optical Methods?

Destructive woody-to-total area ratio was the best woody components correction method amongst the three woody components correction methods in obtaining the LAI with the smallest RMSE and MAE, followed by MCI woody-to-total area ratio (Tables 5, 7, and 9). By contrast, the woody components correction method of obtaining WAI from leaf-off DHP or MCI or DCP images was the worst method for deriving an LAI with the largest RMSE and MAE in most cases (Tables 5, 7, and 9). As expected, destructive woody-to-total area ratio was the best woody components correction method as they were obtained based on the destructive woody-to-total area ratio measurements of representative trees of each plot, which were usually regarded as the highly accurate woody-to-total area ratio estimates compared with those obtained from indirect methods [14,23,55]. The small differences between the RMSE or MAE of the LAIs obtained from DHP using the same Ω_e or Ω_w algorithm and inversion model but with MCI and destructive woody-to-total area ratio measurements (Table 5) illustrate that MCI is an effective and relatively accurate solution to correct the overestimation of the woody components on the LAI estimation from DHP. Compared with the destructive method, MCI has the advantage of low cost, high efficiency, and non-destructiveness to canopies. Thus, MCI can be adopted as the routine option for deriving the woody-to-total area ratio values of *L. principis-rupprechtii* forests.

The PAI obtained from the leaf-on DHP images only using Miller and the three Ω_e algorithms was systematically smaller than those obtained by summing the LAIs derived from the leaf-on DHP images using the same inversion model and Ω_e algorithm with MCI woody-to-total area ratio and the WAI obtained from the leaf-off DHP images using the same inversion model and Ω_w algorithm (Figure 6). This finding is consistent with the finding of Calders et al. [56], although different tree species were covered in the two studies. The differences between the derived PAI of the two calculation methods were mainly attributed to the preferential shading of woody components by the shoots in the canopies. The preferential shading of woody components by shoots would increase the $p_w(\theta)$ and reduce the

WAI and PAI obtained from the leaf-on DHP images as they should be [56]. Zou et al. [23] reported that the proportions of woody components shaded by shoots were large at the zenith angles ranging from 0° to 80° with a 10° interval (7%–73%) in the five leaf-on plots of this study. Therefore, if the WAI derived from the leaf-off DHP images was used as the woody components correction method, then the contribution of woody components to the LAI estimation would be overcorrected as the PAI, which was obtained from the leaf-on DHP images containing a certain degree of WAI underestimation due to the preferential shading of woody components by the shoots in the canopies. This condition also explains why the LAIs obtained from leaf-on and leaf-off measurements were obviously smaller than those derived from the leaf-on measurements regardless of the optical methods, inversion models, and Ω_e or Ω_w algorithm used in the estimation (Tables 4, 6, and 8). Therefore, the WAI obtained from the leaf-off measurements is not recommended as the woody components correction method in the LAI estimation. Caution is required when adopting the WAI obtained from the leaf-off measurements as the woody components correction method in the LAI estimation even this method was frequently adopted in previous studies, such as Cutini et al. [57], Breda [17], Ryu et al. [35], and Toda et al. [58].

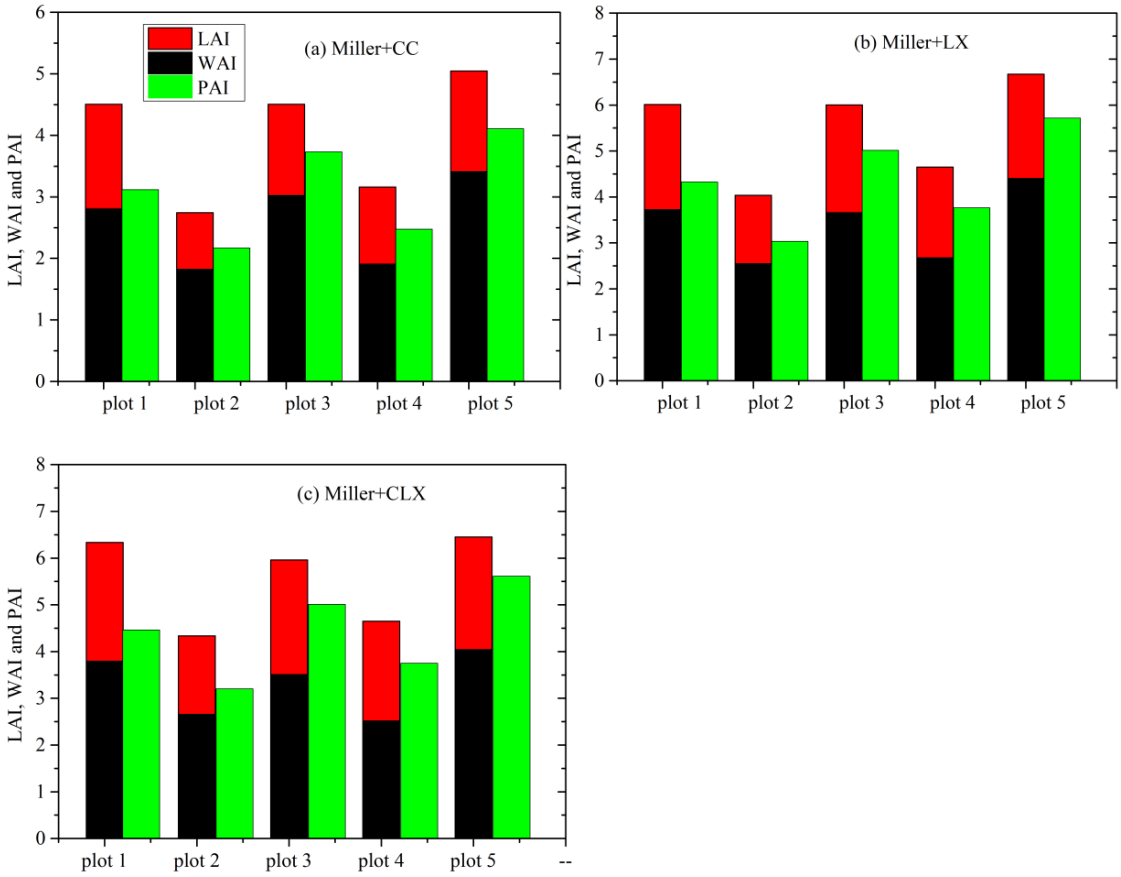

Figure 6. Comparison of two methods of deriving the PAIs of the five leaf-on plots. One method calculates the PAI of the leaf-on plots using the sum of the LAIs obtained from the leaf-on DHP images using Miller, MCI woody-to-total area ratio, and the three canopy element clumping index (Ω_e) algorithms and the WAI derived from the leaf-off DHP images using the same inversion model and Ω_w algorithm (PAI = LAI + WAI). The other method calculates the PAI from the leaf-on DHP images using Miller and the three Ω_e algorithms. Only the results of Miller are shown here as the results of LAI-2200 and Beer show similar behaviors. Similarly, the results of MCI and DCP also show similar behaviors as DHP.

5.3. Which Optical Method(s) Is (Are) More Reliable to Obtain the LAI of L. principis-rupprechtii Forest Plots?

On the basis of TAbles 5, 7, 9 and Figure 5, TRAC and MCI are recommended for use in obtaining the ESU LAI of *L. principis-rupprechtii* forests followed by DHP. DCP is not recommended because it results in obvious LAI underestimation. Given that DCP can sample the canopies sufficiently due to its high image resolution and the large sample size of the sampling scheme (16), accurate $p_e(0)$ or $p_w(0)$ and gap measurements can be obtained from DCP. Therefore, the assumption of the spherical angle distribution of the canopy element made in this study would be the key reason for the LAI underestimation of DCP. On the other hand, the LAI underestimation for DCP indicates that the canopy element and woody components projection coefficients of *L. principis-rupprechtii* forests at 0° obviously deviated from 0.5, which was also observed for forests with other tree species [59,60]. Macfarlane et al. [41] and Chianucci et al. [34] reported that accurate ESU LAI estimates can be obtained from DCP in broad-leaved forests because of two reasons. Firstly, the leaf angle distribution of the forests in the studies of Macfarlane et al. [41] and Chianucci et al. [34] approached spherical distribution. Secondly, the estimates derived from DCP in the two studies were PAIs and not LAIs. Good agreement was found between the PAI and LAI obtained through the litter collection method or allometric equation in the two studies [34,41]. Therefore, if woody components were considered in the LAI estimation, then DCP would underestimate the ESU LAI of forests in the two studies [34,41]. Thus, when the field collected leaf or shoot angle distributions are not available, caution is needed if DCP is adopted in estimating the ESU LAI of forests.

The $p_e(\theta)$ or $p_w(\theta)$ of MCI tends to be smaller than those of DHP and DCP in the five plots (Figures 1 and 2) because of two reasons. Firstly, the isolated shoots and branches in the visible band of the MCI or DHP images tended to be easily overexposed due to the high contrast between the canopy element and the sky (Figure 7a). However, the contrast between the canopy element and the sky or cloud in the near-infrared band of MCI is relatively small (Figure 7b) [61]. Secondly, the shoots have a low reflectance in the visible band due to the strong absorption by chlorophyll, a relatively high reflectance in the near-infrared band due to the internal leaf scattering, and no absorption [62]. Consequently, the shoot sizes in the near-infrared band were larger than those in the visible band for the same shoot (Figure 7a,b). This issue was not carefully considered by the "IsoData" classification algorithm adopted in the MCI image classification.

MCI was originally designed to obtain the woody-to-total area ratio values of forests [14,23]. Compared with DHP, MCI has two advantages in the ESU LAI estimation of forests. Firstly, the ESU LAI of forests can be derived from this single method without the combination of any other optical method due to its ability to discriminate between leaves or shoots, woody components, and sky [14]. Secondly, the forest canopies can be sufficiently sampled by MCI at all zenith directions of the hemisphere due to its high image resolution and hemispherical sampling scheme [14]. MCI also has two disadvantages in ESU LAI estimation. Firstly, MCI is a proprietary device and is unavailable as a commercial instrument for scientists compared with LAI-2200 and TRAC. Secondly, great effort and a large amount of resources are needed to collect and process the MCI images. For example, 54 or 60 measurements (6 measurements for each zenithal direction) and 1 measurement must be collected at each sampling point for MCI [14,23] and DHP, respectively. It is encouraging that the two disadvantages of MCI can be overcome as follows: (1) The charge couple devices of consumer-level cameras have an imaging capability in the near-infrared band after removing the infrared blocking filter before the charge couple devices [63]. Then, consumer-level cameras can be modified following the procedures described in Chapman [63] to obtain the visible and near-infrared band images of forests similar to MCI with the combination of filters. (2) Given that relatively accurate woody-to-total area ratio measurements [23] and LAI can be derived from MCI using Beer (Table 7), the Beer inversion model can be used to derive the ESU LAI of forests, and then only those MCI images with a zenith angle near 57° should be collected to reduce the effort and resources needed for MCI.

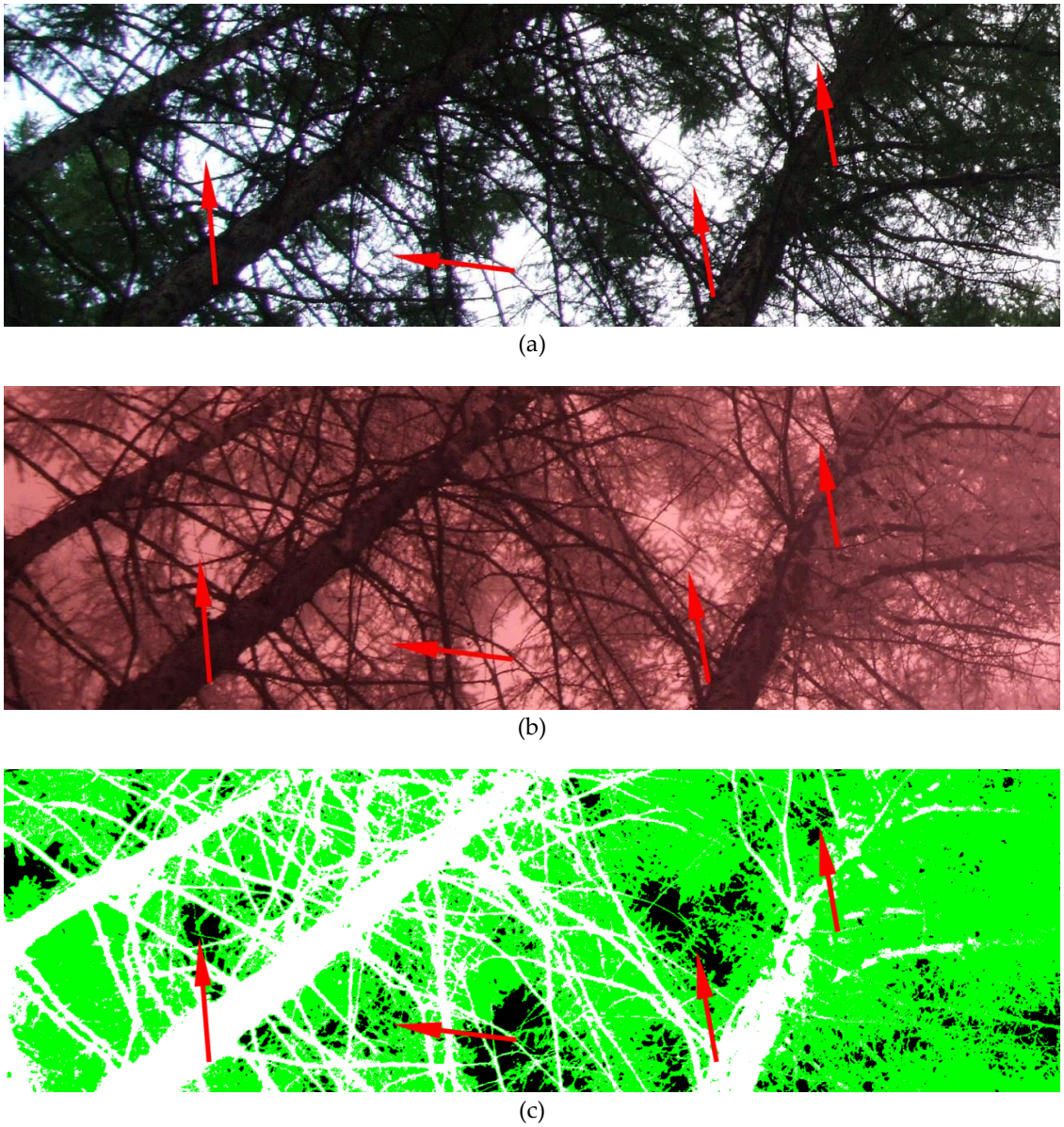

Figure 7. An example of the visible (**a**) and near-infrared (**b**) band images of one MCI image pair collected at one sampling point with azimuthal and zenith angles of 0° and 20° in plot 1, respectively (only half of the original images are shown here to improve the readership). (**c**) shows the corresponding classified MCI image of the MCI image pair.

The $p_e(\theta)$ or $p_w(\theta)$ of TRAC tended to be smaller than those of MCI, DHP, and DCP (Figures 1 and 2). This finding is consistent with the finding of Raabe et al. [64], Leblanc et al. [32], Pisek et al. [33], and Ryu et al. [35]. This can be attributed to the limitation of TRAC sensor resolution as the small within canopy gaps were underestimated by TRAC [64]. For TRAC, a problem occurred when the LAI-2200 or Miller inversion model was adopted by TRAC in the ESU LAI estimation because only one $p_e(\theta)$ or $p_w(\theta)$ and $\Omega_e(\theta)$ or $\Omega_w(\theta)$ estimate can be obtained from each TRAC measurement. In practice, the TRAC measurement datasets of each plot with the same zenith angle range covered by LAI-2200 or Miller are difficult to gather, especially for plots in high latitude areas where the solar zenith angles of daytime are usually small. An alternative option for TRAC to be adopted as the routine method in the LAI estimation is to derive the LAI with the combination of TRAC and Beer. Similar Ω_w estimates were obtained from MCI and TRAC (0.90 and 0.94) at a zenith angle of 64° in the leaf-off plot 3, indicating that TRAC remains effective in deriving Ω_w at this zenith angle (Figure 8). However,

Law et al. [65] suggested avoiding taking TRAC measurements at zenith angles larger than 60° due to the difficulty of TRAC to distinguish small gaps at these zenith angles. An error Ω_e estimate of 0.75 was derived at zenith angle of 75° for TRAC in the leaf-on plot 5 as all the photosynthetic photon flux density values of this TRAC measurement was equal to zero μmol m^{-2} s^{-1} (not shown in Figure 4). Therefore, caution is needed for TRAC to derive the Ω_e or Ω_w and LAI of *L. principis-rupprechtii* forests at zenith angles larger than 70°.

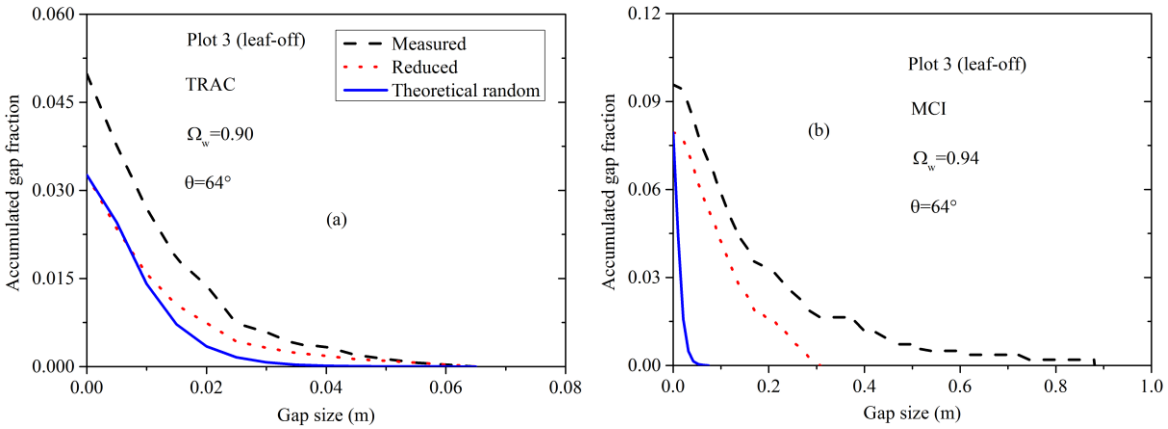

Figure 8. An example of the measured, reduced, and theoretical random accumulated gap size distributions obtained from TRAC and MCI in leaf-off plot 3 (**a**,**b**), respectively.

Two reasons contributed to the ESU LAI underestimation for DHP in the five forests [47]. Firstly, previous studies reported that the gap fraction measurements of optical methods tended to be saturated at forests with large LAIs due to canopy closure, especially for forests with LAIs ~ > 5.0–6.0 [16,47,55]. Secondly, the $\Omega_e(\theta)$ or $\Omega_w(\theta)$ of DHP was larger than that of MCI in the five leaf-on or leaf-off plots in most cases (Figures 3 and 4), indicating that DHP overestimated the Ω_e or Ω_w estimates in the five leaf-on or leaf-off plots because the Ω_e or Ω_w estimation of DHP suffered from the two error sources of canopy sampling and mean element width estimation.

Compared with TRAC, MCI, and DCP, DHP has the advantage of obtaining the hemispherical direction measurements of $p_e(\theta)$ or $p_w(\theta)$ and $\Omega_e(\theta)$ or $\Omega_w(\theta)$ simultaneously from single or several DHP images. Therefore, less effort and resources are required for DHP than the other three optical methods in the ESU LAI estimation of forests. DHP is frequently used as the routine method for obtaining the ESU LAI of forests. However, the performance of DHP in deriving the ESU LAI of the five forests was strongly affected by the inversion model, Ω_e or Ω_w algorithm and woody components correction method adopted in the estimation (Tables 4 and 5). This finding is consistent with the finding of Liu et al. [24], Zou et al. [19], and van Gardingen et al. [66] who reported large differences between the LAIs derived from DHP using various inversion models, Ω_e or Ω_w algorithms and woody components correction methods. Therefore, the best combination of inversion model, Ω_e or Ω_w algorithm and woody components correction method should be identified before DHP is selected as the routine method to estimate the ESU LAI of forests.

5.4. Do the Four Optical Methods Qualify to Obtain the ESU LAI of Forests with the Accuracy Match the Requirements of GCOS?

Table 5 indicates that the LAI of DHP with the smallest MAE (21%) was obtained using Miller, CLX and destructive woody-to-total area ratio. This result indicates that DHP is not qualified to derive the ESU LAI of *L. principis-rupprechtii* forests with estimation errors of <5% or 20% required by GCOS. However, the LAI with the MAEs <20% can be obtained from DHP in the five *L. principis-rupprechtii* forests using Miller, CLX and destructive woody-to-total area ratio by optimizing the sampling schemes reported by Zou et al. [47]. An LAI MAE range of 11%–16.4% was obtained from DHP when Miller,

CLX, and destructive woody-to-total area ratio in addition to two sampling schemes with the sample sizes in the range of 3–9 were adopted in the ESU LAI estimation of the five plots except plot 5 [47]. This point illustrates that DHP is qualified to derive the ESU LAI of *L. principis-rupprechtii* forests with estimation errors of <20% if the inversion model, Ω_e or Ω_w algorithm and woody components correction method in addition to sampling scheme are considered in the estimation. The LAI MAE range of 11%–16.4% is near that in the study by Leblanc and Fournier [20] who reported a minimum MAE of 11% for the PAI derived from DHP when an appropriate inversion model and Ω_e algorithm are adopted in the PAI estimation of the simulated forest scenes. The LAI MAE range of 11%–16.4% is larger than the minimum PAI MAE in the study of Leblanc and Fournier [20] because the LAI estimation from the field-collected DHP images suffered from three additional estimation errors (i.e., observation conditions, DHP image classification, and woody components correction method) compared with those in the simulation study [47].

Table 5 indicates that DHP is not qualified to derive the ESU LAI of *L. principis-rupprechtii* forests with estimation errors of <5%. Table 9 shows that DCP is not qualified to derive the ESU LAI of *L. principis-rupprechtii* forests with estimation errors of <5% or 20%. Unlike DCP and DHP, MCI and TRAC are qualified to derive the ESU LAI of *L. principis-rupprechtii* forests with estimation errors of <20% (Table 7 and Figure 5). Moreover, TRAC shows the potential in obtaining the ESU LAI of *L. principis-rupprechtii* forests with estimation errors of <5% (Figure 5).

6. Conclusions

In this study, the performance of four optical methods (i.e., DHP, DCP, TRAC, and MCI) in estimating the ESU LAI of *L. principis-rupprechtii* forests was evaluated using the LAIs obtained from litter collection measurements. The impact of three factors (i.e., inversion model, Ω_e or Ω_w algorithm, and woody components correction method) on the LAI estimation was analyzed. Results show that the ESU LAI estimation was largely affected by the three factors. To obtain accurate ESU LAIs of *L. principis-rupprechtii* forests, we suggest the following procedures:

(1) using MCI and TRAC as the ESU LAI estimation methods;
(2) using CC to derive the Ω_e or Ω_w;
(3) using the destructive or MCI woody-to-total area ratio as the woody components correction method;
(4) using the Beer inversion model to derive the ESU LAI.

The accuracies of ESU LAIs obtained by the four optical methods were evaluated in terms of whether they matched the LAI accuracy target required by GCOS. Results show that the four optical methods, except for DCP, could obtain the ESU LAI of *L. principis-rupprechtii* forests with an MAE of <20% required by GCOS. Only TRAC shows potential in obtaining the ESU LAI of *L. principis-rupprechtii* forests with an MAE of <5%.

Given the limited efforts and resources available, only five plots were covered in this study. More plots should be covered in the future to improve the conclusions drawn in this study and evaluate whether management activities (e.g., branches harvesting and thinning) and the LAI range of the plots are factors that affect the performance of the four optical methods for deriving the ESU LAI of *L. principis-rupprechtii* forests. Future work could include efforts to evaluate the performance of a commonly used method of LAI-2200 in the ESU LAI estimation of *L. principis-rupprechtii* forests.

Author Contributions: Conceptualization, J.Z.; Methodology, J.Z.; Software, J.Z.; Investigation, J.Z., P.L.; Data Curation, J.Z., Y.Z., P.Z., and W.H.; Writing-Original Draft Preparation, J.Z.; Writing-Review & Editing, J.Z., B.C.; Visualization, J.Z.; Funding Acquisition, J.Z. All authors have read and agreed to the published version of the manuscript.

Funding: This work was jointly funded by the National Key Research and Development Program from Ministry of Science and Technology of China (2016YFB0501501) and National Natural Science Foundation of China (Grant Nos. 41871233, 41371330, and 41001203).

Conflicts of Interest: The authors declare no conflict of interest.

Abbreviations

List of Symbols [19,47]

A_n	half the total needle area in a shoot
$A_p(0°, 0°)$	shoot projection area measured by projecting shoot at zenith angle 0° and azimuth angle 0°
$A_p(45°, 0°)$	shoot projection area measured by projecting shoot at zenith angle 45° and azimuth angle 0°
$A_p(90°, 0°)$	shoot projection area measured by projecting shoot at zenith angle 90° and azimuth angle 0°
Beer	Beer inversion model (Equations (8) and (12))
CC	gap size distribution algorithm
CLX	combination of gap size and logarithmic averaging algorithm
DBH	diameter at breast height
DCP	digital cover photography
DHP	digital hemispherical photography
ESU	elementary sampling unit
$F_m(0, \theta)$	measured total canopy element gap fraction at θ
$F_{mr}(0, \theta)$	total canopy element gap fraction after removing large gaps resulting from non-random distribution of canopy element at θ
f_c	crown cover
f_f	foliage cover
GCOS	global climate observing system
G_e	canopy element projection coefficient
$G_e(\theta)$	canopy element projection coefficient at θ
G_{e_i}	canopy element projection coefficient of ith annulus
LAI	leaf area index
LAI_{Beer}	leaf area index estimated using the Beer inversion model
$LAI_{LAI-2200}$	leaf area index estimated using modified Miller theorem of LAI-2200 instrument
LAI_{Miller}	leaf area index estimated using Miller theorem
LAI_{DCP}	leaf area index estimated from digital cover photography method
LAI-2200	LAI-2200 inversion model (Equations (10) and (14))
$\overline{ln[p_e(\theta)]}$	mean logarithmic canopy element gap fraction for all segments at θ
LX	logarithmic averaging algorithm
MAE	mean absolute error
MCI	multispectral canopy imager
MCI_0-85	modified Miller integration similar to calculation method of LAI-2200 instrument for MCI
Miller	Miller theorem (Equations (9) and (13))
$p_e(\theta)$	canopy element gap fraction at θ
$\overline{p_e(\theta)}$	mean canopy element gap fraction of all segments at θ
$p_{e\_i}(\theta_i)$	canopy element gap fraction of ith annulus
$p_{e\_k}(\theta)$	canopy element gap fraction of segment k at θ
$p_w(\theta)$	woody components gap fraction at θ
$p_{w\_i}(\theta_i)$	woody components gap fraction of ith annulus
PAI	plant area index
PAI_{Beer}	plant area index estimated using Beer inversion model
$PAI_{LAI-2200}$	plant area index estimated using modified Miller theorem of LAI-2200 instrument
PAI_{MCI_0-85}	plant area index estimated using the MCI_0-85 inversion model
PAI_{Miller}	plant area index estimated using Miller theorem

RMSE	root mean square error
TRAC	tracing radiation of canopy and architecture method
WAI	woody area index
W_i	weight of ith annulus
θ	zenith angle
θ_i	centre zenith angle of ith annulus
α	woody-to-total area ratio
α_i	α of i^{th} annulus of MCI, which were derived using CC
α_{DCP}	mean α_i of first and second annuli of MCI, which were derived using CC
γ	needle-to-shoot area ratio
γ_c	corrected needle-to-shoot area ratio
n	number of segments
Ω_e	canopy element clumping index
Ω_{e_i}	Ω_e of ith annulus
$\Omega_e(\theta)$	canopy element clumping index at θ
$\Omega_{e\_CC}(\theta)$	canopy element clumping index estimated using gap size distribution algorithm at θ
$\Omega_{e\_CC\_k}(\theta)$	Ω_e of segment k at θ
$\Omega_{e\_DCP}(0)$	canopy element clumping index estimated from digital cover photography
$\Omega_{e\_LX}(\theta)$	canopy element clumping index estimated using logarithmic averaging algorithm at θ
$\Omega_{e\_CLX}(\theta)$	canopy element clumping index estimated using a combination of gap size and logarithmic averaging algorithm at θ
Ω_w	woody components clumping index
$\Omega_w(\theta)$	woody components clumping index at θ
$\varnothing$	crown porosity

References

1. Fang, H.; Baret, F.; Plummer, S.; Schaepman-Strub, G. An overview of global leaf area index (lai): Methods, products, validation, and applications. *Rev. Geophys.* **2019**, *57*, 739–799. [CrossRef]
2. Fernandes, R.; Plummer, S.; Nightingale, J.; Baret, F.; Camacho, F.; Fang, H.; Garrigues, S.; Gobron, N.; Lang, M.; Lacaze, R.; et al. *Global Leaf Area Index Product Validation Good Practices (Version 2.0)*; Land Product Validation Subgroup (WGCV/CEOS): Roma, Italy, 2014. [CrossRef]
3. Baret, F.; Hagolle, O.; Geiger, B.; Bicheron, P.; Miras, B.; Huc, M.; Berthelot, B.; Niño, F.; Weiss, M.; Samain, O.; et al. Lai, fapar and fcover cyclopes global products derived from vegetation: Part 1: Principles of the algorithm. *Remote Sens. Environ.* **2007**, *110*, 275–286. [CrossRef]
4. Masson, V.; Champeaux, J.-L.; Chauvin, F.; Meriguet, C.; Lacaze, R. A global database of land surface parameters at 1-km resolution in meteorological and climate models. *J. Clim.* **2003**, *16*, 1261–1282. [CrossRef]
5. Feng, D.; Chen, J.M.; Plummer, S.; Mingzhen, C.; Pisek, J. Algorithm for global leaf area index retrieval using satellite imagery. *IEEE Trans. Geosci. Remote Sens.* **2006**, *44*, 2219–2229. [CrossRef]
6. Xiao, Z.; Liang, S.; Wang, J.; Chen, P.; Yin, X.; Zhang, L.; Song, J. Use of general regression neural networks for generating the glass leaf area index product from time-series modis surface reflectance. *IEEE Trans. Geosci. Remote Sens.* **2014**, *52*, 209–223. [CrossRef]
7. Knyazikhin, Y.; Martonchik, J.V.; Myneni, R.B.; Diner, D.J.; Running, S.W. Synergistic algorithm for estimating vegetation canopy leaf area index and fraction of absorbed photosynthetically active radiation from modis and misr data. *J. Geophys. Res. Atmos.* **1998**, *103*, 32257–32275. [CrossRef]
8. Wenze, Y.; Dong, H.; Bin, T.; Stroeve, J.C.; Shabanov, N.V.; Knyazikhin, Y.; Nemani, R.R.; Myneni, R.B. Analysis of leaf area index and fraction of par absorbed by vegetation products from the terra modis sensor: 2000–2005. *IEEE Trans. Geosci. Remote Sens.* **2006**, *44*, 1829–1842. [CrossRef]
9. Baret, F.; Weiss, M.; Lacaze, R.; Camacho, F.; Makhmara, H.; Pacholcyzk, P.; Smets, B. Geov1: Lai and fapar essential climate variables and fcover global time series capitalizing over existing products. Part1: Principles of development and production. *Remote Sens. Environ.* **2013**, *137*, 299–309. [CrossRef]
10. Fang, H.; Jiang, C.; Li, W.; Wei, S.; Baret, F.; Chen, J.M.; Garcia-Haro, J.; Liang, S.; Liu, R.; Myneni, R.B.; et al. Characterization and intercomparison of global moderate resolution leaf area index (lai) products: Analysis of climatologies and theoretical uncertainties. *J. Geophys. Res. Biogeosci.* **2013**, *118*, 529–548. [CrossRef]

11. Garrigues, S.; Lacaze, R.; Baret, F.; Morisette, J.T.; Weiss, M.; Nickeson, J.E.; Fernandes, R.; Plummer, S.; Shabanov, N.V.; Myneni, R.B.; et al. Validation and intercomparison of global leaf area index products derived from remote sensing data. *J. Geophys. Res. Biogeosci.* **2008**, *113*. [CrossRef]
12. Jingming, C. Remote sensing of leaf area index of vegetation covers. In *Remote Sensing of Natural Resources*; Weng, Q., Ed.; CRC Press: Boca Raton, FL, USA, 2014; p. 24.
13. Yang, X.; Zhiqiang, X.; Shunlin, L.; Jindi, W.; Jinlin, S. Validation of global land surface satellite (glass) leaf area index product. *J. Remote Sens.* **2014**, *18*, 573–596.
14. Zou, J.; Yan, G.; Zhu, L.; Zhang, W. Woody-to-total area ratio determination with a multispectral canopy imager. *Tree Physiol.* **2009**, *29*, 1069–1080. [CrossRef] [PubMed]
15. Woodgate, W. In-situ leaf area index estimate uncertainty in forests: Supporting earth observation product calibration and validation. Ph.D. Thesis, RMIT University, Melbourne, Australia, 2015.
16. Jonckheere, I.; Fleck, S.; Nackaerts, K.; Muys, B.; Coppin, P.; Weiss, M.; Baret, F. Review of methods for in situ leaf area index determination: Part i. Theories, sensors and hemispherical photography. *Agric. For. Meteorol.* **2004**, *121*, 19–35. [CrossRef]
17. Bréda, N.J.J. Ground-based measurements of leaf area index: A review of methods, instruments and current controversies. *J. Exp. Bot.* **2003**, *54*, 2403–2417. [CrossRef]
18. Weiss, M.; Baret, F.; Smith, G.J.; Jonckheere, I.; Coppin, P. Review of methods for in situ leaf area index (lai) determination: Part ii. Estimation of lai, errors and sampling. *Agric. For. Meteorol.* **2004**, *121*, 37–53. [CrossRef]
19. Zou, J.; Zhuang, Y.; Chianucci, F.; Mai, C.; Lin, W.; Leng, P.; Luo, S.; Yan, B. Comparison of seven inversion models for estimating plant and woody area indices of leaf-on and leaf-off forest canopy using explicit 3d forest scenes. *Remote Sens.* **2018**, *10*, 1297. [CrossRef]
20. Leblanc, S.G.; Fournier, R.A. Hemispherical photography simulations with an architectural model to assess retrieval of leaf area index. *Agric. For. Meteorol.* **2014**, *194*, 64–76. [CrossRef]
21. Macfarlane, C. Classification method of mixed pixels does not affect canopy metrics from digital images of forest overstorey. *Agric. For. Meteorol.* **2011**, *151*, 833–840. [CrossRef]
22. Cao, B.; Du, Y.; Li, J.; Li, H.; Li, L.; Zhang, Y.; Zou, J.; Liu, Q. Comparison of five slope correction methods for leaf area index estimation from hemispherical photography. *IEEE Geosci. Remote Sens. Lett.* **2015**, *12*, 1958–1962. [CrossRef]
23. Zou, J.; Leng, P.; Hou, W.; Zhong, P.; Chen, L.; Mai, C.; Qian, Y.; Zuo, Y. Evaluating two optical methods of woody-to-total area ratio with destructive measurements at five *larix gmelinii* rupr. Forest plots in China. *Forests* **2018**, *9*, 746. [CrossRef]
24. Liu, Z.; Jin, G.; Chen, J.; Qi, Y. Evaluating optical measurements of leaf area index against litter collection in a mixed broadleaved-korean pine forest in China. *Trees* **2015**, *29*, 59–73. [CrossRef]
25. Ma, L.; Zheng, G.; Eitel, J.U.H.; Magney, T.S.; Moskal, L.M. Determining woody-to-total area ratio using terrestrial laser scanning (tls). *Agric. For. Meteorol.* **2016**, *228–229*, 217–228. [CrossRef]
26. Zhu, X.; Skidmore, A.K.; Wang, T.; Liu, J.; Darvishzadeh, R.; Shi, Y.; Premier, J.; Heurich, M. Improving leaf area index (lai) estimation by correcting for clumping and woody effects using terrestrial laser scanning. *Agric. For. Meteorol.* **2018**, *263*, 276–286. [CrossRef]
27. Camacho, F.; Cernicharo, J.; Lacaze, R.; Baret, F.; Weiss, M. Geov1: Lai, fapar essential climate variables and fcover global time series capitalizing over existing products. Part 2: Validation and intercomparison with reference products. *Remote Sens. Environ.* **2013**, *137*, 310–329. [CrossRef]
28. Baret, F.; Weiss, M.; Allard, D.; Garrigue, S.; Leroy, M.; Jeanjean, H.; Fernandes, R.; Myneni, R. VALERI: A Network of Sites and a Methodology for the Validation of Medium Spatial Resolution Satellite Products. 2005. Available online: w3.avignon.inra.fr/valeri/documents/VALERI-RSESubmitted.pdf (accessed on 18 October 2019).
29. Campbell, J.L.; Burrows, S.; Gower, S.T.; Cohen, W.B. Bigfoot field manual (version 2.1). 1999. Available online: https://daac.ornl.gov/cgi-bin/dataset_lister.pl?p=1 (accessed on 18 October 2019).
30. Swap, R.J.; Annegarn, H.J.; Suttles, J.T.; Haywood, J.; Helmlinger, M.C.; Hely, C.; Hobbs, P.V.; Holben, B.N.; Ji, J.; King, M.D.; et al. The southern african regional science initiative (safari 2000): Overview of the dry season field campaign. *S. Afr. J. Sci.* **2002**, *98*, 125–130.
31. Gonsamo, A.; Pellikka, P. The computation of foliage clumping index using hemispherical photography. *Agric. For. Meteorol.* **2009**, *149*, 1781–1787. [CrossRef]

32. Leblanc, S.G.; Chen, J.M.; Fernandes, R.; Deering, D.W.; Conley, A. Methodology comparison for canopy structure parameters extraction from digital hemispherical photography in boreal forests. *Agric. For. Meteorol.* **2005**, *129*, 187–207. [CrossRef]
33. Pisek, J.; Lang, M.; Nilson, T.; Korhonen, L.; Karu, H. Comparison of methods for measuring gap size distribution and canopy nonrandomness at järvselja rami (radiation transfer model intercomparison) test sites. *Agric. For. Meteorol.* **2011**, *151*, 365–377. [CrossRef]
34. Chianucci, F.; Cutini, A. Estimation of canopy properties in deciduous forests with digital hemispherical and cover photography. *Agric. For. Meteorol.* **2013**, *168*, 130–139. [CrossRef]
35. Ryu, Y.; Sonnentag, O.; Nilson, T.; Vargas, R.; Kobayashi, H.; Wenk, R.; Baldocchi, D.D. How to quantify tree leaf area index in an open savanna ecosystem: A multi-instrument and multi-model approach. *Agric. For. Meteorol.* **2010**, *150*, 63–76. [CrossRef]
36. Chen, J.M.; Rich, P.M.; Gower, S.T.; Norman, J.M.; Plummer, S. Leaf area index of boreal forests: Theory, techniques, and measurements. *J. Geophys. Res. Atmos.* **1997**, *102*, 29429–29443. [CrossRef]
37. Lang, A.R.G.; Yueqin, X. Estimation of leaf area index from transmission of direct sunlight in discontinuous canopies. *Agric. For. Meteorol.* **1986**, *37*, 229–243. [CrossRef]
38. Walter, J.-M.N.; Fournier, R.A.; Soudani, K.; Meyer, E. Integrating clumping effects in forest canopy structure: An assessment through hemispherical photographs. *Can. J. Remote Sens.* **2003**, *29*, 388–410. [CrossRef]
39. Chen, J.M.; Cihlar, J. Plant canopy gap-size analysis theory for improving optical measurements of leaf-area index. *Appl. Opt.* **1995**, *34*, 6211–6222. [CrossRef]
40. Chen, J.M.; Cihlar, J. Quantifying the effect of canopy architecture on optical measurements of leaf area index using two gap size analysis methods. *IEEE Trans. Geosci. Remote Sens.* **1995**, *33*, 777–787. [CrossRef]
41. Macfarlane, C.; Hoffman, M.; Eamus, D.; Kerp, N.; Higginson, S.; McMurtrie, R.; Adams, M. Estimation of leaf area index in eucalypt forest using digital photography. *Agric. For. Meteorol.* **2007**, *143*, 176–188. [CrossRef]
42. Chen, J.M. Optically-based methods for measuring seasonal variation of leaf area index in boreal conifer stands. *Agric. For. Meteorol.* **1996**, *80*, 135–163. [CrossRef]
43. Leblanc, S.G. Correction to the plant canopy gap-size analysis theory used by the tracing radiation and architecture of canopies instrument. *Appl. Opt.* **2002**, *41*, 7667–7670. [CrossRef]
44. Nilson, T. A theoretical analysis of the frequency of gaps in plant stands. *Agric. For. Meteorol.* **1971**, *8*, 25–38. [CrossRef]
45. Miller, J. A formula for average foliage density. *Aust. J. Bot.* **1967**, *15*, 141–144. [CrossRef]
46. LI-COR. *Lai-2200 Plant Canopy Analyzer Instruction Manual*; Li-cor Cor.: Lincoln, NE, USA, 2009.
47. Zou, J.; Hou, W.; Zhong, P.; Zuo, Y.; Luo, S.; Leng, P. Evaluating the impact of sampling schemes on leaf area index measurements from digital hemispherical photography in *Larix principis-rupprechtii* Forest plots. *For. Ecol. Manag.* **2019**, submitted.
48. Sun, Z.; Liu, L.; Peng, S.; Peñuelas, J.; Zeng, H.; Piao, S. Age-related modulation of the nitrogen resorption efficiency response to growth requirements and soil nitrogen availability in a temperate pine plantation. *Ecosystems* **2016**, *19*, 698–709. [CrossRef]
49. Yan, T.; Lü, X.-T.; Zhu, J.-J.; Yang, K.; Yu, L.-Z.; Gao, T. Changes in nitrogen and phosphorus cycling suggest a transition to phosphorus limitation with the stand development of larch plantations. *Plant Soil* **2018**, *422*, 385–396. [CrossRef]
50. Deng, M.; Liu, L.; Sun, Z.; Piao, S.; Ma, Y.; Chen, Y.; Wang, J.; Qiao, C.; Wang, X.; Li, P. Increased phosphate uptake but not resorption alleviates phosphorus deficiency induced by nitrogen deposition in temperate *larix principis-rupprechtii* plantations. *New Phytol.* **2016**, *212*, 1019–1029. [CrossRef] [PubMed]
51. Gonsamo, A.; Pellikka, P. Methodology comparison for slope correction in canopy leaf area index estimation using hemispherical photography. *For. Ecol. Manag.* **2008**, *256*, 749–759. [CrossRef]
52. Zou, J.; Yan, G.; Chen, L. Estimation of canopy and woody components clumping indices at three mature *Picea crassifolia* forest stands. *IEEE J. Sel. Top. Appl. Earth Obs. Remote Sens.* **2015**, *8*, 1413–1422. [CrossRef]
53. Leblanc, S.G.; Chen, J.M.; Kwong, M. *Tracing Radiation and Architecture of Canopies Trac Manual (Version 2.1.3)*; Natural Resources Canada: Ottawa, ON, Canada, 2002; p. 25.
54. Gonsamo, A.; Walter, J.-M.N.; Pellikka, P. Sampling gap fraction and size for estimating leaf area and clumping indices from hemispherical photographs. *Can. J. Forest Res.* **2010**, *40*, 1588–1603. [CrossRef]

55. Gower, S.T.; Kucharik, C.J.; Norman, J.M. Direct and indirect estimation of leaf area index, fapar, and net primary production of terrestrial ecosystems. *Remote Sens. Environ.* **1999**, *70*, 29–51. [CrossRef]
56. Calders, K.; Origo, N.; Disney, M.; Nightingale, J.; Woodgate, W.; Armston, J.; Lewis, P. Variability and bias in active and passive ground-based measurements of effective plant, wood and leaf area index. *Agric. For. Meteorol.* **2018**, *252*, 231–240. [CrossRef]
57. Cutini, A.; Matteucci, G.; Mugnozza, G.S. Estimation of leaf area index with the li-cor LAI-2000 in deciduous forests. *For. Ecol. Manag.* **1998**, *105*, 55–65. [CrossRef]
58. Toda, M.; Richardson, A.D. Estimation of plant area index and phenological transition dates from digital repeat photography and radiometric approaches in a hardwood forest in the northeastern united states. *Agric. For. Meteorol.* **2018**, *249*, 457–466. [CrossRef]
59. Pisek, J.; Sonnentag, O.; Richardson, A.D.; Mõttus, M. Is the spherical leaf inclination angle distribution a valid assumption for temperate and boreal broadleaf tree species? *Agric. For. Meteorol.* **2013**, *169*, 186–194. [CrossRef]
60. Raabe, K.; Pisek, J.; Sonnentag, O.; Annuk, K. Variations of leaf inclination angle distribution with height over the growing season and light exposure for eight broadleaf tree species. *Agric. For. Meteorol.* **2015**, *214–215*, 2–11. [CrossRef]
61. Kucharik, C.J.; Norman, J.M.; Murdock, L.M.; Gower, S.T. Characterizing canopy nonrandomness with a multiband vegetation imager (mvi). *J. Geophys. Res. Atmos.* **1997**, *102*, 29455–29473. [CrossRef]
62. Knipling, E.B. Physical and physiological basis for the reflectance of visible and near-infrared radiation from vegetation. *Remote Sens. Environ.* **1970**, *1*, 155–159. [CrossRef]
63. Chapman, L. Potential applications of near infra-red hemispherical imagery in forest environments. *Agric. For. Meteorol.* **2007**, *143*, 151–156. [CrossRef]
64. Raabe, K.; Pisek, J.; Lang, M.; Korhonen, L. Estimating the beyond-shoot foliage clumping at two contrasting points in the growing season using a variety of field-based methods. *Trees* **2017**, *31*, 1367–1373. [CrossRef]
65. Law, B.E.; Van Tuyl, S.; Cescatti, A.; Baldocchi, D.D. Estimation of leaf area index in open-canopy ponderosa pine forests at different successional stages and management regimes in oregon. *Agric. For. Meteorol.* **2001**, *108*, 1–14. [CrossRef]
66. van Gardingen, P.R.; Jackson, G.E.; Hernandez-Daumas, S.; Russell, G.; Sharp, L. Leaf area index estimates obtained for clumped canopies using hemispherical photography. *Agric. For. Meteorol.* **1999**, *94*, 243–257. [CrossRef]